Comparing Model Representations of Physiological Limits on Transpiration at a Semi-arid Ponderosa Pine Site

Linnia R Hawkins[1], Maoya Bassouni[2], William R. L. Anderegg[3], Martin David Venturas[4], Stephen Paul Good[5], Hyojung Kwon[5], Chad Hanson[5], Richard P Fiorella[3], Gabriel Bowen[3], and Christopher J. Still[5]

[1]Forest Ecosystems & Society, Oregon State University
[2]Department of Crop Production Ecology, Swedish University of Agricultural Sciences
[3]University of Utah
[4]Department of Biology, University of Utah
[5]Oregon State University

November 21, 2022

Abstract

Mechanistic representations of biogeochemical processes in ecosystem models are rapidly advancing, requiring advancements in model evaluation approaches. Here we quantify multiple aspects of model functional performance to evaluate improved process representations in ecosystem models. We compare semi-empirical stomatal models with hydraulic constraints against more mechanistic representations of stomatal and hydraulic functioning at a semi-arid pine site using a suite of metrics and analytical tools. We find that models generally perform similarly under unstressed conditions, but performance diverges under atmospheric and soil drought. The more empirical models better capture synergistic information flows between soil water potential and vapor pressure deficit to transpiration, while the more mechanistic models are overly deterministic. Additionally, both multilayer canopy and big-leaf models were unable to capture the magnitude of canopy temperature divergence from air temperature. Lastly, modeled stable carbon isotope fractionation differed under canopy water stress which illustrates the value of carbon isotopes in helping to characterize ecosystem function and elucidate differences attributable to model structure. This study demonstrates the value of merging underutilized observational data streams with emerging analytical tools to characterize ecosystem function and discriminate among model process representations.

Comparing Model Representations of Physiological Limits on Transpiration at a Semi-arid Ponderosa Pine Site

Linnia R. Hawkins[1], Maoya Bassouni[2], William R. L. Anderegg[3], Martin D. Venturas[4], Stephen P. Good[5], Hyojung J. Kwon[1], Chad V. Hanson[1], Richard P. Fiorella[6], Gabriel J. Bowen[6], and Christopher J. Still[1]

[1]Department of Forestry, Oregon State University, Corvallis, OR
[2]Department of Crop Production Ecology, Swedish University of Agricultural Sciences, Uppsala, Sweden
[3]School of Biological Sciences, University of Utah, Salt Lake, UT
[4]Departamento de Sistemas y Recursos Naturales, Universidad Politécnica de Madrid, Madrid, Spain
[5]Department of Biological and Ecological Engineering, Oregon State University, Corvallis, OR
[6]Department of Geology and Geophysics, Unversity of Utah, Salt Lake, UT

Corresponding author: Linnia Hawkins (Linnia.Hawkins@oregonstate.edu)

Key Points:

- We evaluate several model formulations for coupling plant hydraulic and stomatal functioning using functional performance metrics.
- Information flows from soil water potential and vapor pressure deficit to transpiration illustrate functional differences among models.
- Considerable biases in modeled canopy temperature propagate to a 5% offset in cumulative growing season transpiration.

Abstract

Mechanistic representations of biogeochemical processes in ecosystem models are rapidly advancing, requiring advancements in model evaluation approaches. Here we quantify multiple aspects of model functional performance to evaluate improved process representations in ecosystem models. We compare semi-empirical stomatal models with hydraulic constraints against more mechanistic representations of stomatal and hydraulic functioning at a semi-arid pine site using a suite of metrics and analytical tools. We find that models generally perform similarly under unstressed conditions, but performance diverges under atmospheric and soil drought. The more empirical models better capture synergistic information flows between soil water potential and vapor pressure deficit to transpiration, while the more mechanistic models are overly deterministic. Additionally, both multilayer canopy and big-leaf models were unable to capture the magnitude of canopy temperature divergence from air temperature. Lastly, modeled stable carbon isotope fractionation differed under canopy water stress which illustrates the value of carbon isotopes in helping to characterize ecosystem function and elucidate differences attributable to model structure. This study demonstrates the value of merging underutilized observational data streams with emerging analytical tools to characterize ecosystem function and discriminate among model process representations.

Plain Language Summary

Earth system models are an essential tool for understanding the consequences of changing climate conditions on forest ecosystems. Models are rapidly incorporating more realistic representations of how drought impacts ecosystem carbon and water cycling. These advancements need to be thoroughly evaluated to ensure that the models adequately capture the plant functional response to drought stress. Here we merge underutilized measurements with new analytical tools to evaluate several model representations of plant response to drought. These tools allow us to both better understand relationships among drought stress and ecosystem response, as well as quantify model accuracy. We find that models generally perform similarly under unstressed conditions, but performance diverges under atmospheric and soil drought.

1 Introduction

Climate change mitigation, adaptation, and conservation efforts all leverage ecosystem models to understand and predict carbon and water cycling at local to global scales. Ecosystem models have rapidly advanced in recent decades and now incorporate mechanistic representations of many plant and soil processes (e.g., Kennedy et al., 2019; Sabot et al., 2020; Eller et al., 2020). Recent developments have focused on the representation of plant hydraulic functioning to improve mechanistic modeling of water transport through the soil-plant-atmosphere continuum, but how best to represent the effects of drought stress on plant gas-exchange, especially when quantifying ecosystem-scale fluxes, is still an open question (Mencuccini et al., 2019). Evaluating improved plant hydraulic representation in ecosystem models requires more comprehensive frameworks for quantifying model performance, including both metrics for evaluating functional relations among processes, and comparisons against underutilized observational data.

Early land surface models (e.g., Bonan et al., 1995; Cox et al., 1998) implemented an empirical model for stomatal functioning based on gas-exchange measurements (Ball et al., 1987), which has been used for decades with strong empirical support (e.g., Damour et al., 2010; Lin et al., 2015). However, a predominant theory of stomatal functioning (Cowan and Farquhar, 1977) assumes plants optimize stomatal behavior such that the benefit of carbon gained (A*)* is equivalent to the respective cost of water loss by way of transpiration (T). As such, stomata optimize the tradeoff between carbon gain and the carbon cost of transpiration, $A - \lambda T$, where λ (mol CO_2 / mol H_2O) is the carbon cost per unit water used by the plant. This theoretical basis has been used to develop semi-empirical stomatal models (Medlyn et al., 2011), which have been shown to be fundamentally based on the same physiological principles as the Ball et al., (1987) model (Franks et al., 2017).

Many studies have demonstrated that semi-empirical models perform well under well-watered conditions but do not capture soil drought responses correctly (e.g. Powell et al., 2013; Bonan et al., 2014; Medlyn et al., 2016; Ukkola et al., 2016). These semi-empirical models are limited by the need to prescribe a constant value for λ, which does not respond to environmental conditions and is not based on measurable plant traits (Buckley, 2017). Optimization theory supports the

conceptual framework of hydraulic limitation on gas exchange since the cost of hydraulic damage can be incorporated into the cost of water loss. However, there is little consensus on how best to represent hydraulic costs in models.

To directly couple stomatal conductance to plant hydraulic mechanisms, model formulations of optimal stomatal behavior have been proposed that assume plants balance carbon gain against hydraulic risk (e.g. Williams et al., 1996; Sperry et al., 2017; Mencuccini et al., 2019; Wang et al., 2020). The mechanistic optimization models have the advantage of being parameterized with measurable plant traits and have been shown to perform well at the plant scale (e.g., Venturas et al., 2018; Wang et al., 2020). A comparison of different stomatal optimization principles in a big-leaf framework, indicated that formulations with explicit representation of plant hydraulics did not substantially improve ecosystem-scale evapotranspiration estimates (Bassiouni and Vico, 2021). At the ecosystem scale, Sabot et al., (2020) found that the Sperry et al., (2017) model demonstrated improved performance over the Medlyn et al., (2011) model and Bonan et al., (2014) showed that the Soil-Plant-Atmosphere optimization model (Williams et al., 1996) demonstrated some improvement over the Ball et al., (1987) model when water availability was limited. However, both evaluations only compared the more mechanistic models against semi-empirical models without hydraulic constraints. Although there is still much discussion about how hydraulic functioning should be applied in semi-empirical models (Lin et al., 2015), hydraulic limitations have been incorporated into semi-empirical stomatal models (Tuzet et al., 2003; Zhou et al., 2013; Wolf et al., 2016; Xu et al., 2016; Yang et al., 2019; Kennedy et al., 2019).

Here we compare semi-empirical models with hydraulic constraints against more mechanistic optimization models at the ecosystem scale. We implement hydraulic constraints within the Ball et al., (1987) and Medlyn et al., (2011) models by altering the water use efficiency parameter as a function of the leaf water potential. We evaluate these hydraulic-modified semi-empirical models against two mechanistic approaches. One approach was developed by Williams et al., (1996) in the soil-plant-atmosphere model (SPA) where the stomatal conductance is calculated to optimize water-use efficiency while avoiding hydraulic failure. This model conceptualizes hydraulic failure by a simple minimum leaf water potential threshold. Another approach we evaluate here is the Sperry et al., (2017) model of optimal stomatal behavior which assumes

plants maximize carbon gain while avoiding hydraulic risk. This model integrates across xylem elements to determine the hydraulic vulnerability at an instantaneous drop in canopy water potential.

Model intercomparisons are commonly performed by benchmarking the mean state and variability of simulated carbon and water fluxes against observations (e.g. Kennedy et al., 2019; Sabot et al., 2020). But it is particularly important to ensure that the functional relationships among environmental conditions and ecosystem responses are also adequately captured (Kirchner, 2006; Ruddell et al., 2019; Bassiouni & Vico, 2021), particularly when models are intended to make future projections. We leverage ecosystem-scale measurements from a long running intensively monitored AmeriFlux core site in a seasonally drought stressed ecosystem and employ a suite of diagnostics designed to disentangle physiological limits on transpiration. We evaluate the influence of different model process representations on the simulated functional relationships among meteorological conditions, soil water availability, and transpiration at diurnal to daily time scales and for a range of atmospheric and/or soil water stressed conditions. This study demonstrates the value of merging observational data and novel analytical tools to characterize ecosystem function and discriminate among model representations.

2 Methods

2.1 Site and observational data description

The Metolius forest study site is in a mature coniferous forest in central Oregon at an elevation of 1253 m asl. The forest is a core research site in the AmeriFlux network (site US-Me2) where microclimate and eddy-covariance flux measurements are collected from a flux tower. The canopy is dominated by ponderosa pine trees (*Pinus ponderosa*) with scattered incense cedars (*Calocedrus decurrens*). Trees are evenly distributed with a leaf area index (LAI) of 2.8 (m^2 leaf m^{-2} ground). Tree height is relatively homogeneous at about 18 m, and the mean tree density is approximately 339 trees ha^{-1} (Irvine et al., 2008). The climate is semi-arid, with warm and dry summers and cool and wet winters, with most precipitation occurring as snow or rain during the winter and spring (November through April). Additional descriptions of the study site, as well as information on site instrumentation and measurements, can be found in Law et al. (2001), Irvine

et al., (2004), Thomas et al., (2009) and Ruehr et al., (2014). In this study, we examine the period of 2006-01-01 to 2018-12-31 where the observational records of data streams overlap. We define the growing season as May 1st to August 31st which coincides with the warmest and driest months of the year at this site.

The US-Me2 site is instrumented with a 33m tower measuring above canopy eddy-covariance fluxes of CO_2, H_2O, latent and sensible heat. Mature ponderosas have been instrumented with sapflow probes which are used to estimate whole tree transpiration by scaling with estimates of sapwood area (see Kwon et al., 2018). We also calculate the canopy conductance per unit ground area (G_c, mm/s) from the sapflow estimates of transpiration, air temperature (T_a, °C), and vapor pressure deficit (VPD, kPa) using a simplified form of the Penman-Monteith equation as suggested by Monteith and Unsworth (1990) as is typically used in ecohydrological studies (Kwon et al., 2018). Canopy temperature was also measured in 2015 (Kim et al., 2016) using a thermal camera (FLIR A325sc). The thermal camera measured the temperature of the upper canopy and we averaged over a selected area of interest to represent only canopy foliage. Soil probes measure soil water content at 10, 20, 30, 50, 70, 100, 130, 160cm depths (Sentek Technologies, Stepney, SA, Australia). We calculated the root weighted soil water potential using the relationship between soil water content and water retention from Ruehr et al., (2014) and the root profile prescribed in the SPA model (Table 1).

2.2 SPA multi-layer canopy model description

The Soil-Plant-Atmosphere model (SPA; Williams et al., 1996, 2001a) is a high vertical resolution point model (up to 10 canopy layers and 20 soil layers) which simulates exchanges of carbon, water, and energy between the land surface and atmosphere on sub-hourly timesteps. The SPA model has been used for a variety of applications including site level analyses of carbon and water fluxes (Williams et al., 1996, 2001a, 2001b; Ruehr et al., 2014); model intercomparisons of stomatal and hydraulic functioning (Misson et al., 2004; Bonan et al., 2014); data assimilation (Williams et al., 2005; Sus et al., 2014); and modeling land-atmosphere feedbacks (Hill et al., 2008; Smallman et al., 2013). In this study, we implemented several model updates including

those from a recent study which used the SPA model to simulate the carbon cycle at US-Me2 under current and future climate conditions (Ruehr et al., 2014).

The SPA model includes a detailed radiative transfer scheme for long-wave, near infra-red, and direct and diffuse photosynthetically active radiation to determine transmittance, reflectance, and absorption in each canopy layer for sunlit and shaded leaf fractions. Leaf energy balance is coupled to a widely used biochemical model of photosynthesis (Farquhar and von Caemmerer, 1982) and leaf transpiration through an optimization scheme for stomatal conductance. In this study's implementation, rather than using the Penman-Monteith equation for leaf transpiration, we calculated transpiration directly from Fick's law as:

$$T = g_w * D_l \quad (1)$$

where T is the transpiration rate per unit leaf area (mmol m^{-2} s^{-1}), g_w is the two-sided leaf total conductance (series of stomatal and leaf boundary layer) to water vapor (mmol m^{-2} s^{-1}), and D_l is the leaf-specific vapor deficit (mol mol^{-1}).

The SPA model calculates stomatal conductance for each canopy layer based on a hypothesis that stomatal conductance is regulated to prevent hydraulic failure (Williams et al., 1996, 2001a). The transport of water through the soil-plant-atmosphere continuum flows down a potential gradient at a rate proportional to the whole-plant conductance. The plant conductance is a static function of hydraulic architecture, xylem construction, and leaf conductance and the soil-to-root conductance is a function of soil hydraulic conductivity and root density. Following Ruehr et al., (2014), we reduced whole plant conductance in response to declining soil water potential according to a sigmoid function and reduced the soil tortuosity and soil surface roughness length to increase soil water evaporation and better match observations.

In this application, we used six canopy layers, each with equivalent LAI but varied thickness to approximate canopy structure (Reinhardt et al., 2006). The vertical soil profile was defined by 20 soil layers of 0.1m thickness with soil texture defined as in Law et al., (2001). We modified the SPA model to run using prescribed soil water content and implemented a site-specific empirical relationship between soil water content and soil water potential following Ruehr et al., (2014). Configuration of canopy structure, photosynthesis parameters, and rooting profile can be found

211 in Table 1, and we provide more information on model updates in the Supplementary
212 Information.
213

Model	Description	Units	Value	Source
All	Leaf area index	m^2 m^{-2}	2.8	Irvine et al., 2004
All	Leaf carbon per leaf area	gC m^{-2} leaf area	122.4	Ruehr et al., 2014
All	Maximum rooting depth	m	1.1	Ruehr et al., 2014
All	Total root biomass	g m^{-2}	70	Ruehr et al., 2014
All	Vcmax at 25°C	umol m^{-2} s^{-1}	31.4	Ruehr et al., 2014
All	Jmax at 25°C	umol m^{-2} s^{-1}	52.4	Ruehr et al., 2014
All	Canopy height	m	18	Ruehr et al., 2014
SPA	Height of canopy layers	m	18,15.9,15.1,14.2,13.3,11.8,9	defined to have equal LAI and follow canopy structure.
SPA	Average foliar nitrogen	gN m^{-2} leaf area	2.1	Schwarz et al., 2004
SPA	Plant capacitance	mmolH2O m^{-2} leaf area MPa^{-1}	2500	Bonan et al., 2014
SPA	Root resistivity	MPa s g $mmol^{-1}$	20	Ruehr et al., 2014
Gain-Risk	Leaf area:basal area	m^2 m^{-2}	878	Irvine et al., 2004
Gain-Risk	Basal area:ground area	m^2 Ha^{-1}	31.9	Irvine et al., 2004
Gain-Risk	Rhizosphere resistivity	(%)	50	Venturas et al., 2018

214 **Table 1.** Canopy structure, root distribution and photosynthesis parameter values used in models.
215
216 *2.3 Stomatal sub-models in SPA*
217
218 We compared four sub-models with unique assumptions regarding stomatal behavior within the
219 SPA model framework, each including explicit hydraulic mechanisms that down regulate
220 stomatal conductance in response to more negative plant water potential. We implemented
221 hydraulic constraints to the Ball et al., (1987) model (hereafter referred to as BB-H) and the
222 Medlyn et al., (2011) model (MED-H); and use two different definitions of stomatal efficiency in

the SPA optimization scheme based on intrinsic water use efficiency (WUEi) and the ratio of CO_2 assimilation to transpiration (WUE).

The predominant semi-empirical model for stomatal functioning was developed by Ball et al., (1987) who defined a simple linear approximation of the relationship between photosynthesis and stomatal conductance to water (g_w; mol H_2O m^{-2} s^{-1}) based on gas exchange data:

$$g_w = g_0 + g_{1B}\left(\frac{A*rh}{C_a}\right) \quad (2)$$

where A is the net assimilation rate (μmol CO_2 m^{-2} s^{-1}), rh is the relative humidity at the leaf surface (mol mol^{-1}), C_a is the atmospheric CO_2 concentration at the leaf surface (μmol mol^{-1}) and g_0 and g_{1B} are fitted parameters. While g_0 and g_{1B} are determined by fitting the equation to leaf-gas exchange data, both represent physiologically meaningful quantities (Franks et al., 2017). The intercept parameter, g_0, is the minimum stomatal conductance and is usually close to zero. We set g_0 to 0.1 as in Franks et al., (2017) throughout this study. The slope parameter, g_{1B}, is generally representative of g_w/A, the reciprocal of the intrinsic water use efficiency, A/g_w (Farquhar, 1989; Feng et al., 1999). The Ball et al., (1987) model assumes that stomata respond to relative humidity at the leaf level, but it is more likely that stomata sense water fluxes (Aphalo & Jarvis, 1991) and respond to changes in water status of the leaf tissue (Buckley, 2005; 2019).

An alternative framework for stomatal function was developed by Cowan and Farquhar (1977) based on the premise that optimal stomatal behavior maximizes carbon gain minus the carbon cost of water loss, $A - \lambda E$, where λ is often defined as the water use efficiency. By combining theory of optimal stomatal control (Cowan & Farquhar, 1977) and photosynthesis (Farquhar et al., 1980), Medlyn et al., (2011) derived the following expression for stomatal conductance:

$$g_w = g_0 + 1.6\left(1 + \frac{g_{1M}}{\sqrt{VPD}}\right)\frac{A}{C_a} \quad (3)$$

Where VPD is the vapor pressure deficit (kPa), and g_0 and g_{1M} are fit parameters. Despite having a similar form to the Ball et al., (1987) model, the fit parameter g_{1M} in the Medlyn et al., (2011) model has a different theoretical interpretation: g_{1M} is proportional to the marginal water cost of carbon (λ) and the CO_2 compensation point (Γ):

$$g_{1M} = \sqrt{\frac{3\Gamma\lambda}{1.6}} \quad (4)$$

In this application, we introduce a hydraulic constraint into the Ball et al., (1987) and Medlyn et al., (2011) stomatal models similarly to the approach of Wolf et al., (2016). At short time scales, λ is usually treated as an unknown fitted constant but λ can also be determined from system boundary conditions and generally follows an exponential function with soil moisture (Cowan 1986, Mäkelä et al., 1986; Manzoni et al., 2013), therefore supporting our semi-empirical model variations. Specifically, the instantaneous leaf water potential in each canopy layer modifies the g_1 parameter according to a Weibull function based on the leaf hydraulic vulnerability curve as:

$$g_1 = g_{1_0} * e^{-\left(\frac{-LWP}{b}\right)^c} \quad (5)$$

Where g_{1_0} is the value of g_1 when soil water potential is near zero, LWP represents the instantaneous leaf water potential (MPa), and the Weibull *b* and *c* parameters are fitted according to measurements of ponderosa pine hydraulic leaf hydraulic vulnerability (Figure S1). Hereafter we refer to the Ball et al., (1987) and Medlyn et al., (2011) models with hydraulic constraints as BB-H and MED-H, respectively.

In the default SPA model, stomatal conductance shares some commonalities with theory of optimal stomatal behavior (Cowan & Farquhar, 1977). Stomatal conductance is calculated to maximize assimilation, given transport of water from soil-to-leaf, plant water storage, and hydraulic safety margins (Figure 1). The optimization scheme incrementally increases stomatal aperture until further opening either: 1) does not increase carbon gain per unit water loss (defined by the stomatal efficiency parameter); or 2) causes leaf water potential to drop below a pre-set minimum value (*minLWP*). The stomatal efficiency is defined as the assimilation divided by the stomatal conductance to water (A/g_w) and we refer to this version of the SPA model as WUEi. Bonan et al., (2014) introduced an alternate definition of stomatal efficiency into the SPA model, A/T, which we refer to as WUE. Both implementations can represent conservative to more intensive plant water use behavior. For example, conservative behavior is achieved by setting a higher stomatal efficiency value and increasing the amount of appreciable carbon gain per unit increase in stomatal opening. As a result, excessive transpiration is avoided in the morning when atmospheric demand is low in order to preserve water to buffer the effects of high mid-day atmospheric demands (i.e., more isohydric behavior). Low values of stomatal efficiency result in intensive water use (higher optimal g_w and more transpiration).

283 *2.4 Gain-Risk big-leaf model description*

284

285 We also applied the model of Sperry et al., (2017), a big-leaf model with five soil layers
286 (hereafter referred to as the Gain-Risk model). Stomatal functioning in the Gain-Risk model is
287 based on optimization theory and assumes plants maximize carbon gain while minimizing
288 hydraulic risk (Sperry & Love, 2015; Sperry et al., 2016, 2017; Wolf et al., 2016; Anderegg et
289 al., 2018). The resulting coordination between stomatal and xylem functioning agrees well with
290 observations (Meinzer et al., 2009) and more strongly agrees with leaf-level gas exchange data
291 than the classic Cowan-Farquhar based optimization models (Anderegg et al. 2018; Wang et al.
292 2020). Carbon gain is calculated as in the SPA model (Farquhar et al., 1980) and the carbon gain
293 function, α, is defined at a given value of T as:

294 $$\alpha = \frac{A_{net}}{A_{max}} \quad (6)$$

295 Hydraulic risk is defined as the fractional loss of hydraulic conductance. Vulnerability to
296 cavitation curves (VC's) for each xylem element (roots, stem, and leaves) are represented by
297 two-parameter Weibull functions:

298 $$K = K_{max} * e^{-\left(\frac{-p}{b}\right)^c} \quad (7)$$

299

300 Where K is the hydraulic conductance, K_{max} is the maximum hydraulic conductance, p is the
301 pressure imposed on each xylem element, and b and c are fit parameters (Figure S1). At each
302 increment in T, the pressure drop across xylem elements ($p_{up} - p_{down}$) is calculated and the supply
303 function is then defined as the relationship between T and canopy water potential (P):

304 $$T = \int_{P_{up}}^{P_{down}} K(P)dp \quad (8)$$

305 The derivative of the supply function ($K_c = dT/dP$) represents the hydraulic conductivity loss
306 which is at a maximum (K_{cmax}) when $T=0$, and the hydraulic risk function (θ) is defined as the
307 fractional loss in K_c at a given value of T:

308 $$\theta = 1 - \frac{K_c}{K_{cmax}} \quad (9)$$

309 The Gain-Risk model finds the optimal stomatal conductance by incrementing T from zero and
310 calculating the marginal carbon gain, α, given the environmental conditions at that time step.
311 The hydraulic risk is calculated from the change in P and the optimal T rate is that which
312 maximizes the difference between the carbon gain function and the hydraulic risk function. The

stomatal conductance is then calculated from the optimal T and the VPD at that time step as in the SPA model. Fluxes are then scaled from leaf area to basal area to ground area using measurements from Irvine et al., (2004) (Table 1). We ran the Gain-Risk model without xylem refilling to capture permanent losses in hydraulic conductivity that lead to reductions in transpiration and assimilation after a drought. To ensure that soil water stress was identical across models we prescribed soil water potential in the Gain-Risk model from measurements of soil water content and measured soil water retention curves as with the SPA model.

2.5 Parameterization of stomatal sub-models and hydraulic function

We prescribed model parameter values based on plant trait measurements available in the literature rather than best-fit calibrations in order to reflect how formulations may be used in Earth System Models. Additionally, our goal was to ensure that all parameters with the same mechanistic meaning were equivalent. Therefore, differences in model performances better reflect adequacy of model structures versus differences due to varying parameter calibrations.

Franks et al., (2017) demonstrated that equivalent g_1 parameter values for the Ball et al., (1987) and Medlyn et al., (2011) models can be derived as:

$$g_{1B} \approx \frac{1.6}{rh} * \left(1 + \frac{g_{1M}}{\sqrt{vpd}}\right) \quad (10)$$

Additionally, the WUE stomatal efficiency parameter (ι) in the SPA model is equivalent to $1/\lambda$ thus equations 3 and 4 can be used to determine the equivalent value of ι for a given value of the g_{1M} parameter. In this application we set the Medlyn et al., (2011) g_{1M} parameter to 2.35, determined from gas-exchange data in Lin et al., (2015) representing needleleaf plant functional types. We determined g_{1B} and ι from equations 10 and 4, respectively, with air temperature = 25°C, rh = 0.45, and $\Gamma = 40\ \mu mol/mol$ (Table 2). The Gain-Risk model does not have an equivalent parameter since the water use efficiency is diagnosed from the relationship between carbon gain and hydraulic risk.

The Gain-Risk, WUEi and WUE models all use the leaf specific conductance, which was set to 8.2 mmol m^{-2} s^{-1} MPa^{-1} for a Ponderosa pine as per Johnson et al., (2009). The leaf and root

hydraulic vulnerability curves used in the Gain-Risk model were from previous studies of ponderosa pine (Sperry et al., 2019), while the stem VC was measured at the site but agrees well with literature values used by Sperry et al., (2019). Although the BB-H and MED-H approaches impose hydraulic limitation on stomatal functioning differently than the Gain-Risk model, we used consistent Weibull *b* and *c* parameters from the leaf VC in equation 6 (Figure S1).

BB-H	**Parameter**	**Unit**	**Value**	**Range**
g_{1B}	Fit parameter	unitless	14.2	(6, 14)
Weibull b	VC parameter	-MPa	2.8	(1, 5)
Weibull c	VC parameter	unitless	3.7	(1, 5)
MED-H				
g_{1M}	Fit parameter	$kPa^{0.5}$	2.35	(1, 5)
Weibull b	VC parameter	-MPa	2.8	(1, 5)
Weibull c	VC parameter	unitless	3.7	(1, 5)
WUEi/WUE				
gplant	Leaf specific conductance	Mmol m^{-2} s^{-1} MPa^{-1}	8.2	(3, 30)
minLWP	Minimum leaf water potential	MPa	-2	(-5, -1.7)
ι	stomatal efficiency (WUEi: dA/dg_s, WUE: dA/dE)	(umol CO_2 /molH_2O)	0.0135 / 1350	(0.00375,0.03) (375, 3000)
Gain-Risk				
Kmax	Maximum conductivity	Kg h^{-1} MPa^{-1} m^{-2}	120	(43, 424)
LSC	Leaf specific conductance	Mmol m^{-2} s^{-1} MPa^{-1}	8.2	(3, 30)
Weibull b	VC parameter	-MPa (root/stem/leaf)	1.56 / 4 / 2.8	(0.8, 2.2)
Weibull c	VC parameter	unitless (root/stem/leaf)	1.4 / 3.4 / 3.7	(2, 3.5)

Table 2. Stomatal conductance model parameter definitions, values, and perturbation ranges for sensitivity analysis.

In this study we always assumed plants modify stomatal function instantaneously. The original formulations of WUEi, WUE, and Gain-Risk models modify the water use efficiency in response

to hydraulic constraints on instantaneous timescales. For consistency, we made the same assumption in the BB-H and MED-H models by modifying the g_1 parameter based on instantaneous LWP. Though there is insufficient observational evidence to indicate whether stomata respond instantaneously to stimuli, we tested our assumption by comparing simulated canopy conductance using the predawn versus instantaneous LWP to represent slower versus faster responses of water use efficiency to hydraulic stress. We found that the simulated canopy conductance better matched the diurnal shape of the observed canopy conductance when the instantaneous LWP was used (Figure S2). Continuous measurements of canopy water potential are needed to help constrain these processes and inform model representation. Additionally, all models used in this study assumed hydraulic stress only modified stomatal function, but there is ongoing debate on how non-stomatal responses to hydraulic stress should be implemented in ecosystem models (Zhou et al., 2013).

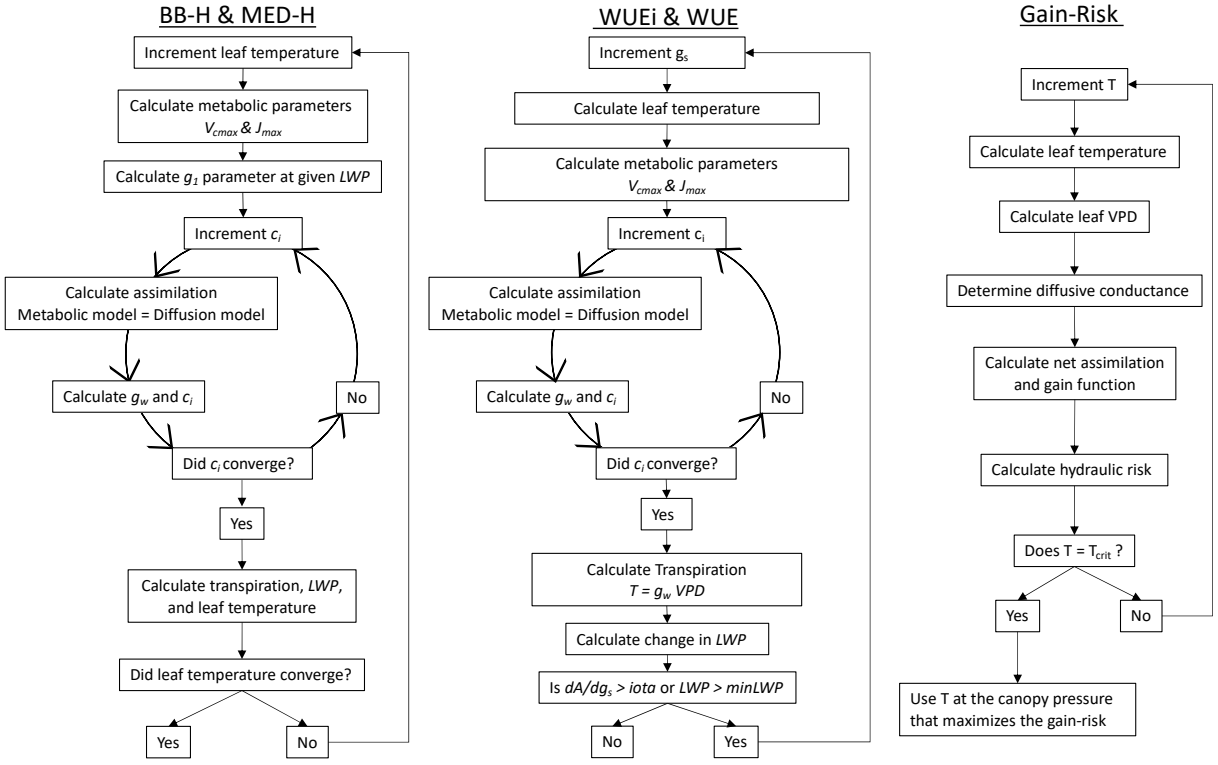

Figure 1. Schematic of leaf flux calculations using the BB-H and MED-H models in the SPA model (left), the WUEi and WUE optimizations in the SPA model (center), and the Gain-Risk model (right).

To elucidate model parameter sensitivity and parameterization uncertainty across models we performed a perturbed parameter experiment. Parameters related to hydraulic and stomatal functioning were modified simultaneously within ranges defined by literature or expert solicitation (Table 2). We performed a Fourier amplitude sensitivity test (FAST; Saltelli and Bolado, 1998) to quantify the contribution of each parameter to the total variance in T. See supplementary information for further description (Text S2, Figures S3, S4).

2.6 Functional performance evaluation

We performed a series of diagnostics to quantify and compare model functional performance under conditions spanning well-watered to atmospheric and/or soil drought stressed. We employed three evaluation strategies, including the analysis of (i) diurnal processes individually; (ii) effective functional relations between processes and an environmental driver; (iii) joint causal relations and functional performance metrics based on information theory. We grouped the data (June–August of 2006–2018) according to inter-quartile ranges of SWP and VPD to examine varying degrees to atmospheric and/or soil water stress. We aggregated SPA leaf-level process simulations over all canopy layers, scaled by the assimilation in the sunlit and shaded fraction of each layer to compare to the ecosystem-scale observations and to maintain consistency with the Gain-Risk model that takes a big-leaf approach (with sunlit and shaded fractions).

We first explored modeled ecosystem-scale processes on diurnal time scales to understand how model assumptions manifest. We compared models in terms of diurnal simulations of transpiration (T); canopy conductance (G_c); canopy water potential (P); gross primary production (GPP); the ratio of internal to external partial pressure of CO_2 (C_i/C_a); and the difference between canopy and air temperature ($T_{can} - T_{air}$). We then compared the simulated diurnal cycle of T under four different levels of atmospheric and/or soil water drought stress to examine how model assumptions affect the diurnal cycle of T in response to environmental stress. We also focused on differences between observed and modeled canopy temperature (T_{can}) because it plays a critical role in the calculation of photosynthetic rates and in the optimization of stomatal conductance. T_{can} can diverge from the air temperature by several degrees, particularly when air temperatures

403 are high (Kim et al., 2016) which can have large consequences for leaf metabolic processes (Still
404 et al., 2019). To illustrate the consequences of T_{can} biases we performed simulations with the
405 MED-H model where we prescribed model leaf temperature as the measured canopy
406 temperature.
407
408 We then evaluated how different model representations influence the sensitivity of G_c to VPD
409 under both low and high soil water stress following Novick et al., (2016). We derived G_c
410 empirically from sapflow and meteorological data and scaled the empirical and modeled G_c
411 estimates by their respective seasonal maximum. We fit an exponential decay function to the
412 rescaled data and compared G_c sensitivity to VPD in observations and models during low water
413 stress days (SWP > 75th percentile) high water stress days (SWP < 25th percentile) separately.
414 We quantified uncertainty in the empirical pattern by modifying the sapflow-derived
415 transpiration by ±40% and re-calculating G_c.
416
417 We also examined differences in model relations between water use efficiency and water
418 potential via C_i/C_a. The ratio C_i/C_a is thought to be a balance point between the stomatal supply
419 and photosynthetic demand for CO_2 and therefore is a measure of water-use efficiency and its
420 response to environmental conditions. C_i/C_a can be inferred from observed ratios of ^{13}C to ^{12}C in
421 cellulose in leaf tissue or tree rings ($\Delta^{13}C$), which have been previously used to constrain model
422 uncertainties (Lavergne et al., 2019). We compared estimated $\Delta^{13}C$ from model simulations
423 using the equation from Farquhar et al., (1982):

424 $$\Delta^{13}\mathrm{C} \approx a + (b - a)\frac{C_i}{C_a} \quad (11)$$

425 where *a* and *b* represent the isotopic fractionations due to diffusion of CO_2 in air (4.4‰) and
426 Rubisco carboxylation (27‰), respectively. Here we exclude the explicit fractionation term for
427 photorespiration and assume infinite boundary layer and mesophyll conductances and negligible
428 fractionation during mitochondrial respiration (Evans and von Caemmerer, 2013).
429
430 We used functional performance metrics based on information theory to quantify the ability of
431 models to reproduce the causal influence of atmospheric water demand and soil water supply
432 together on T as a mapping of inputs to outputs. We therefore evaluated how models represent
433 hydraulic function and feedbacks on gas exchange overall with non-parametric metrics, which

434 are especially relevant because ecosystem-scale data and processes are highly uncertain
435 (Bassiouni and Vico, 2021). Information theory is based on Shannon Entropy (Shannon, 1948), a
436 measure of uncertainty in a random variable or the information required to fully predict that
437 variable. Additionally, mutual information is a measure of the reduction of uncertainty or shared
438 information that knowledge of another variable can provide (Cover & Thomas 2012).
439 Quantifying this shared information among environmental variables, or information flows, has
440 been proven useful in inferring causal interactions among variables in complex ecohydrological
441 systems (Ruddell & Kumar, 2009; Goodwell et al., 2020).
442
443 Specifically, we quantified the information VPD and SWP together provide about observed T.
444 This quantity, the multi-variate mutual information, can be partitioned into four non-negative
445 components (Goodwell and Kumar, 2017) to measure patterns in plant hydraulic controls: unique
446 information (U_{VPD} and U_{SWP}) that only VPD or SWP provide about T; synergistic information
447 (S) that is provided only when both variables are known together; and redundant information (R)
448 that either variable can provide. We therefore evaluated the influence of both VPD and SWP on
449 T which is otherwise challenging to disentangle with established parametric approaches (e.g.,
450 Novick et al., 2016).
451
452 Each model structure may produce the four types (U_{VPD}, U_{SWP}, S, and R) of information
453 differently, and here we quantified model functional performance by comparing information
454 flows in the models to those in the observations at the daily time scale following Bassiouni &
455 Vico, (2021). As such, we calculated six functional performance metrics as the relative
456 difference between observed and modeled total mutual information ($A_{f,T}$); individual
457 information partitioning components ($A_{f,VPD}$, $A_{f,SWP}$, $A_{f,S}$. $A_{f,R}$); and the sum of the absolute
458 values of the partitioning accuracies ($A_{f,P} = |A_{f,SWP}| + |A_{f,VPD}| + |A_{f,S}| + |A_{f,R}|$). Additionally,
459 we quantified predictive performance (A_p) in terms of the relative fraction of missing
460 information about T in the model compared to observations. This metric is calculated as the
461 relative difference between the entropy of observed T and the mutual information between
462 observed and modeled T. We estimated uncertainty by re-calculating the functional performance
463 metrics from 10,000 bootstrapped samples of 80% of the data. For all performance metrics a
464 value of 0 is a perfect match between models and observations.

3 Results

3.1 Diurnal cycle of ecosystem processes

We examined simulated processes on hourly timescales to elucidate how model assumptions manifest in ecological functioning. For illustration, we show simulated days in mid-August 2010 when root-weighted soil water potential was below -1 MPa and daily maximum VPD increased from 1 to nearly 3 kPa (Figure 2). Generally, observed T peaked in the morning and tapered off throughout the day. All models adequately represented the diurnal transpiration except the Gain-Risk model which predicted T peaking in the afternoon. Similarly, observed G_c peaked in the morning and was reduced quickly throughout the day. All models simulated the shape of the diurnal cycle in G_c well, however the magnitude of G_c in the BB-H, MED-H, WUEi, and WUE models was lower than the observed estimate. The Gain-Risk model simulates a slight increase in G_c in the afternoon due to the way G_c is calculated: the model determines the optimal transpiration rate from the Gain-Risk functions, and then stomatal conductance to water vapor, g_w, is calculated as $T=g_w*VPD$. Thus, as transpiration and VPD increase through the day g_w must decline, and as transpiration declines through the afternoon, g_w increases again.

The simulated canopy water potential, P, illustrates the impact of the minimum LWP threshold set in the WUEi and WUE models. Once the threshold is reached the g_w is reduced to avoid cavitation and the minimum LWP is maintained throughout the day. Despite using more sophisticated hydraulic constraint functions, the Gain-Risk model simulates a similar diurnal shape in P. The hydraulic limitation in the BB-H and MED-H models modifies the g_1 parameter as a function of instantaneous LWP; this implementation reduces GPP and T but there are no direct constraints on how low the canopy water potential can get and consequentially the mid-day canopy water potential reaches much lower values compared to the other models.

The magnitude and shape of gross primary productivity (GPP) is well captured by all models; however, the sub-daily variability is not well simulated. All models simulate a much smoother and consistent diurnal cycle of GPP whereas the observations are much more variable. The

simulated ratio of intercellular CO_2 concentration to atmospheric CO_2 concentration (C_i/C_a) often reached minimum values around 0.5 by mid-afternoon.

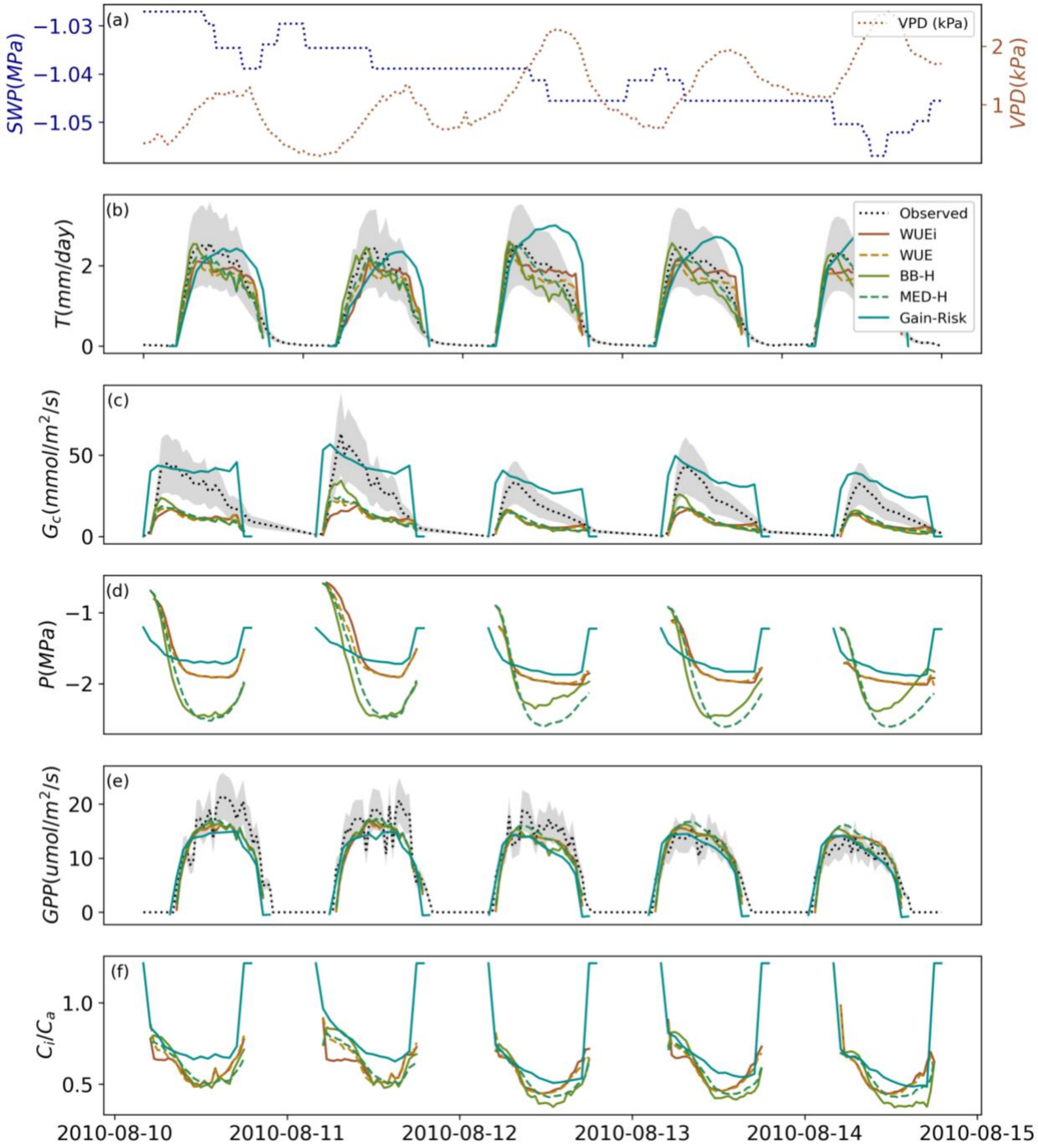

Figure 2. Diurnal cycle of measured or model simulated leaf level processes in mid-August 2010. (a) measured above-canopy VPD (kPa) and root-weighted soil water potential (MPa), (b) transpiration (mm/day) with observations derived from sapflow measurements (black dotted

lines), shading represents uncertainty of ±40% as per Ruehr et al., (2014), (c) canopy conductance (mmol/m^2/s); observations estimated from sapflow measurements (black dotted lines) with shading representing uncertainty in sapflow estimates of transpiration, (d) simulated canopy water potential (MPa); (e) gross primary productivity (umol m^{-2} s^{-1}); and (f) simulated ratio of internal leaf CO_2 to atmospheric CO_2 concentrations.

All models adequately simulated the annual cycle of T and GPP for 2006-2018 (Figure S5) but to better understand model functional performance we evaluated model responses in varying environmental conditions. We assessed how models modify the shape of the diurnal cycle in T in response to VPD and SWP stress, according to four categories: high VPD and low SWP, high VPD and high SWP, low VPD and low SWP, and low VPD and high SWP (Figure 3). Low SWP is more negative and thus indicates higher drought stress. Generally, observed T peaks around 9am and stays relatively constant throughout the day, illustrating the conservative water use strategies typical of ponderosa pines. On days with high VPD there is a midday depression in T, but if soil moisture is not limiting transpiration resumes in the afternoon. All models alter the magnitude and shape of the simulated diurnal cycle in response to VPD and soil water potential, albeit to differing degrees. When soil water stress is high (Figure 3a,c) all models limit mid-day T and shift to more conservative water use. Models show this largest divergence from one another when VPD is high and soil water supply is also high (Figure 3b); high atmospheric demand increases the simulated T (relative to panel d) by varying amounts. Notably, in all categories the diurnal cycle simulated with the Gain-Risk model is markedly different from the observations and the other models. The Gain-Risk model simulates too much T when soil water supply is high (Figure 3b,d) and simulated T peaks in the late afternoon since the VPD constraint on T is applied indirectly via the carbon gain function.

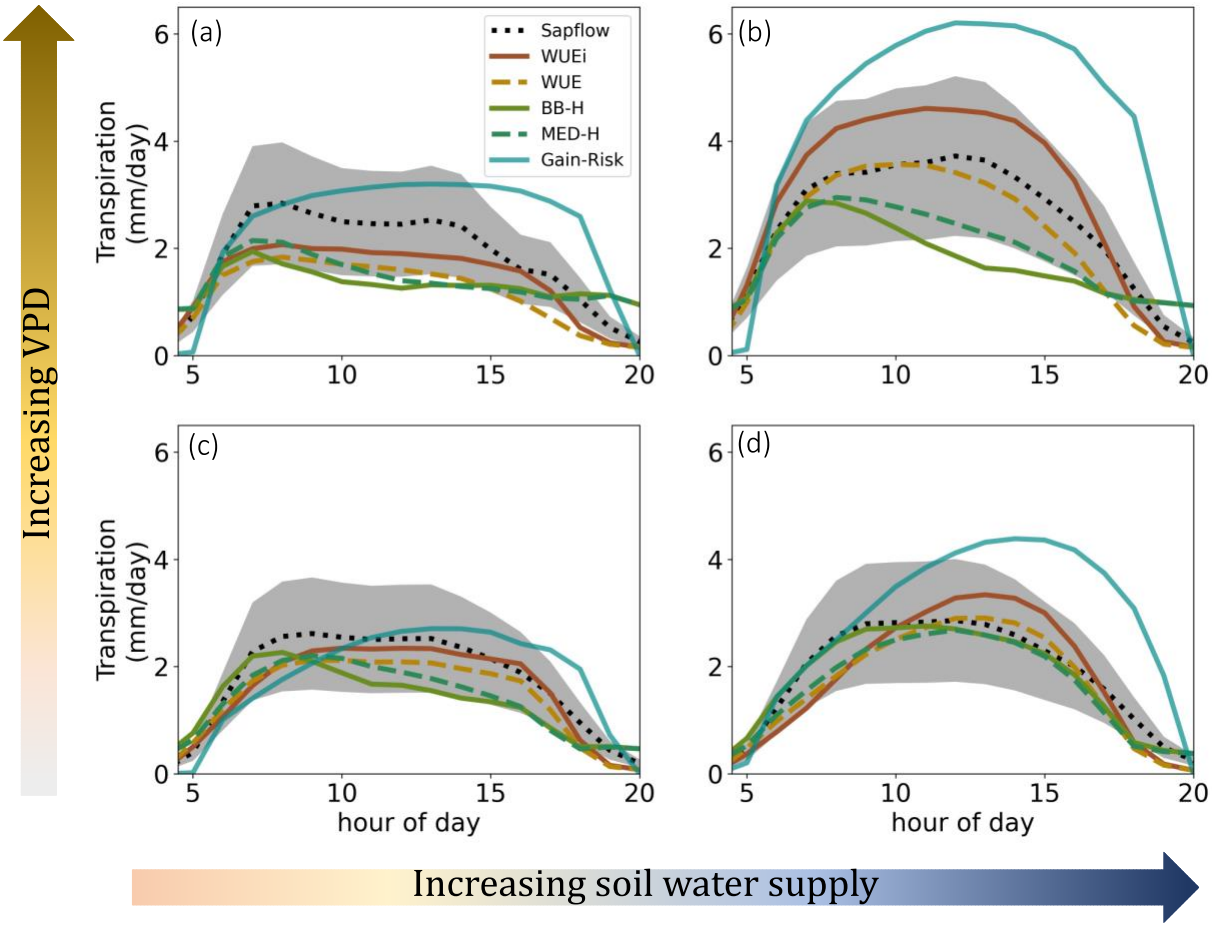

Figure 3. Average diurnal cycle of observed transpiration (black dashed) and modeled transpiration (colors) for days in July (2006–2018) with (a) maximum daily VPD above 75th percentile and root-weighted SWP below 25th percentile (18 days), (b) VPD > 75th percentile and SWP > 50th percentile (41 days) (c) VPD < 50th percentile and SWP < 25th percentile (28 days) and (d) VPD < 50th percentile and SWP > 50th percentile (119 days). Uncertainties in sapflow derived estimates of transpiration are estimated to be 40% (grey shading) as per Ruehr et al., (2014).

3.2 Canopy temperature performance

In August when air temperatures typically peak at this site the observed canopy temperature (T_{can}) diverges from the air temperature (T_{air}) by mid-morning and can be two or three degrees warmer than T_{air} by mid-afternoon (Figure 4a). All models simulate a very slight increase in T_{can} above T_{air} (<1°C) but fail to capture the large observed divergence of T_{can} from T_{air}. The damped

response in modeled leaf temperature persists across models despite different representation of leaf temperature feedback mechanisms. Furthermore, the bias is similar between the multilayer canopy models (SPA) and the big-leaf model (Gain-Risk), which indicates the bias is not ameliorated with increased vertical resolution.

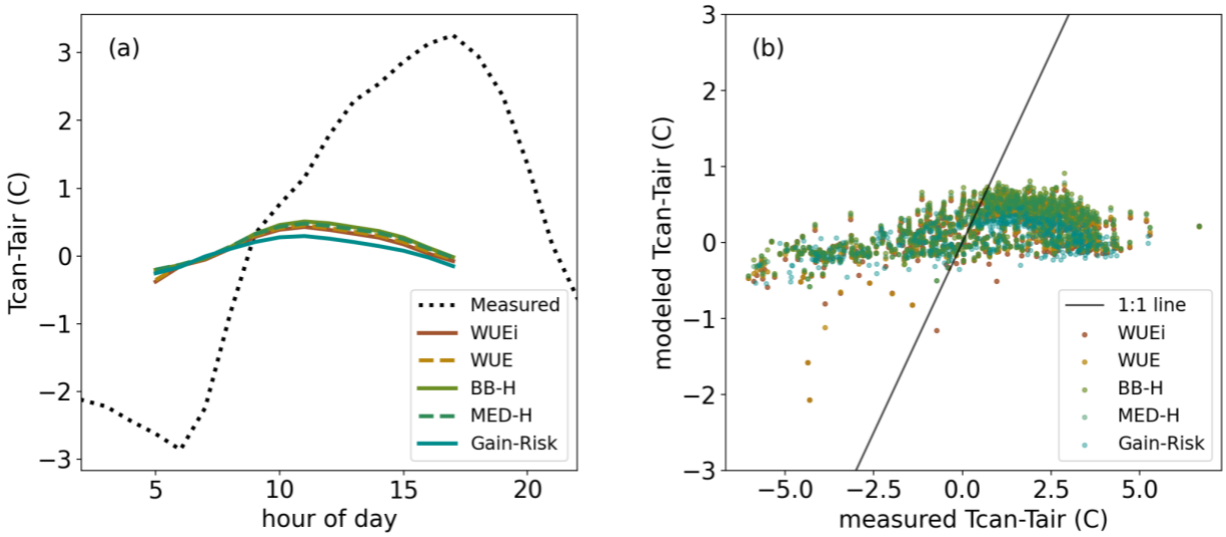

Figure 4. Measured and modeled canopy-air temperature in August 2015. Average diurnal cycle (a) and measured versus modeled daytime mean canopy-air temperature (b).

Prescribing observed leaf temperature in the MED-H model results in cooler morning leaf temperatures and warmer afternoon leaf temperatures (Figure 5a). The cooler morning leaf temperatures lead to more morning transpiration (Figure 5b). In August of 2015, the cumulative morning (8am-12pm) transpiration was 9% higher when using the prescribed canopy temperature. In the afternoons, the prescribed the canopy temperature was warmer than the modeled canopy temperature, which resulted in lower transpiration rates. The cumulative afternoon (12pm-4pm) transpiration in August 2015 was 4% lower when using the prescribed canopy temperature. These results indicate that resolving biases in modeled canopy temperature would lead to increased morning transpiration and decreased afternoon transpiration. These changes counteract one another, and the net effect was a 5% increase in total growing season (JJA) transpiration (not shown).

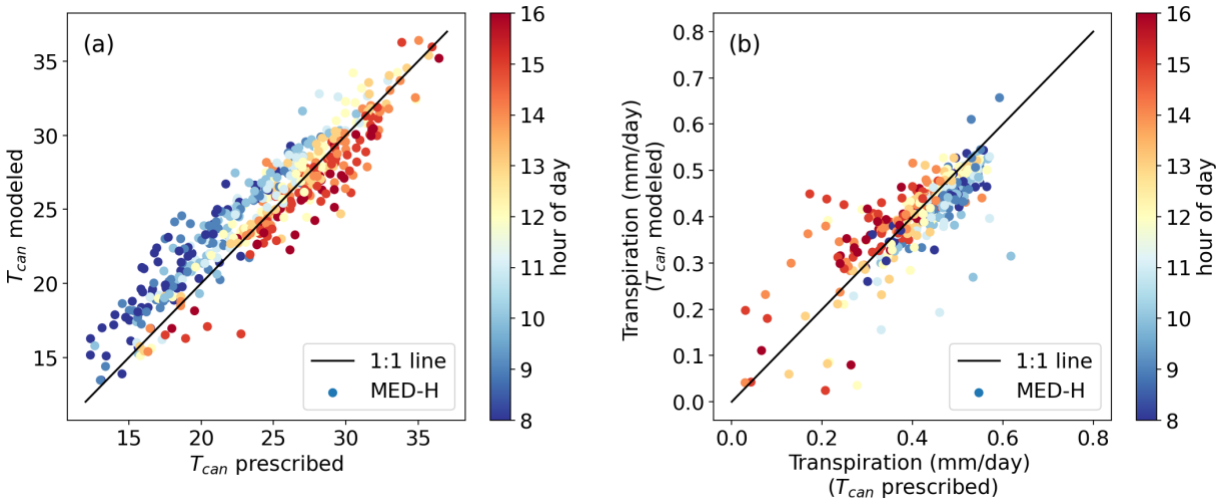

Figure 5. August 2015 canopy temperature (a) and transpiration (b) simulated with the MED-H model using the modeled canopy temperature (y-axis) or the prescribed canopy temperature (x-axis). Shading represents the hour of day; data is shown on 30min time intervals between 8am and 4pm.

3.3 Evaluation of the sensitivity of stomatal conductance to VPD

When water stress was low (SWP above the 75th percentile) the observed G_c had a strong sensitivity to increasing VPD (Figure 6a). None of the models captured the sensitivity to VPD well, all models were less sensitive to VPD than observations. While models were generally indistinguishable, the WUEi model had the lowest sensitivity to VPD. This was expected given that the WUEi model optimizes $\Delta A/\Delta g_s$ and thus does not have a direct dependency on VPD. The WUE optimization has a direct dependency on VPD since stomatal efficiency is defined as $\Delta A/\Delta T$ and thus G_c is more sensitive to VPD as was shown by Bonan et al., (2014). The BB-H and MED-H models have similar sensitivities to VPD even though the MED-H model directly relates g_w to VPD whereas in BB-H g_w is a function of *rh*. However, these results agree well with the findings of Franks et al., (2017) who illustrated that with equivalent parameterizations these two models have similar performance.

When water stress was high (SWP < 25th percentile) the observed G_c was reduced and the sensitivity to VPD was weaker since G_c was already depressed (Figure 6b). The Gain-Risk

583 model captured the magnitude of the depression in G_c when VPD was low, illustrating that soil
584 water potential alone exhibits a strong constraint on G_c in this model. The other models did not
585 depress G_c sufficiently in response to water stress but were more sensitive to VPD, decreasing G_c
586 quickly in response to higher VPD.
587

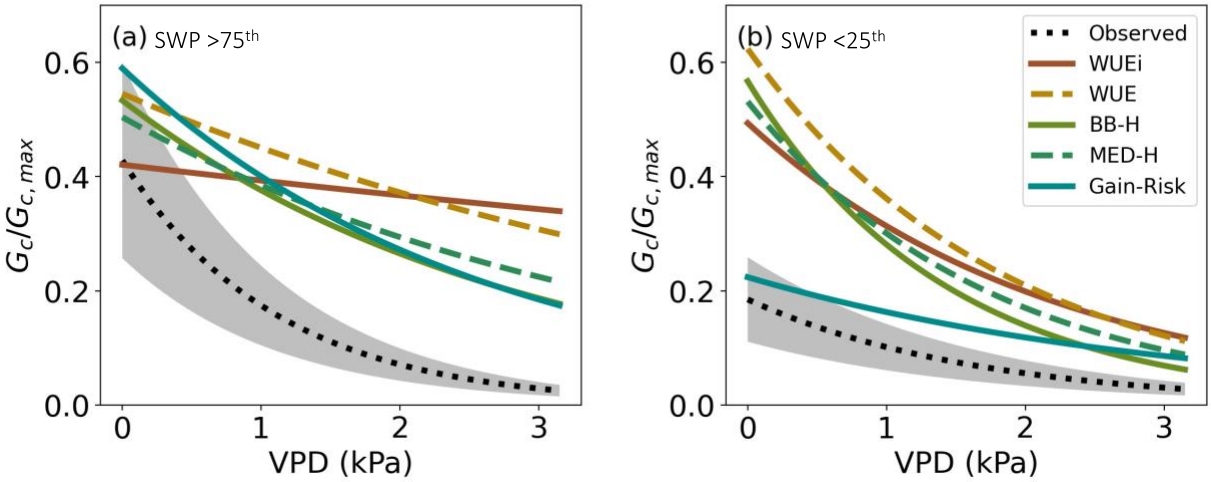

588
589 **Figure 6.** Observed (black) and modeled (color) sensitivity of canopy conductance (G_c/G_{cmax}) to
590 VPD when the soil water potential was greater than the 75th percentile (a), and when the soil
591 water potential was less than the 25th percentile (b). Grey shading represents estimated error in
592 G_c given 40% uncertainty in sapflow-derived transpiration.
593
594 *3.4 Variability in $\Delta^{13}C$ and water stress*
595
596 We examined the simulated monthly mean daytime $\Delta^{13}C$ for June through August 2006–2018.
597 While observational measurements of $\Delta^{13}C$ were not available at this site during the time period
598 covered in this study, we found that the simulated values generally agreed with reported values
599 from the literature. Bowling et al., (2002) reported carbon isotopic composition of ecosystem
600 respiration from a nearby ponderosa site in 1996, 1997 and 2000. Assuming an atmospheric
601 carbon isotope composition of -8‰ the reported values of $\Delta^{13}C$ from Bowling et al., (2002)
602 ranged from 16 to 20‰. Furthermore, they found that $\Delta^{13}C$ decreased non-linearly with
603 increasing VPD. Additionally, Ulrich et al., (2019) determined carbon isotope discrimination at
604 this site using tree-ring cellulose. The reported annual values of $\Delta^{13}C$ for 1990-2002 ranged from
605 17 to 19.5‰, again assuming an atmospheric carbon isotope composition of -8‰.

606

607 We examined simulated $\Delta^{13}C$ to differentiate among model responses to stress. We used the
608 canopy water potential (P) as a measure of plant water stress and compared the simulated
609 response in monthly mean daytime $\Delta^{13}C$ across models (Figure 7a). In the BB-H and MED-H
610 models, $\Delta^{13}C$ decreased linearly with P. The Gain-Risk model also simulated a linear
611 relationship, but $\Delta^{13}C$ declined more rapidly with P indicating that C_i was reduced more quickly
612 under stress. The WUEi and WUE models do not allow P to drop below a threshold (-2 MPa in
613 this study) but the $\Delta^{13}C$ can still be quite low when the minimum P is reached, resulting in an
614 asymptotic relationship. $\Delta^{13}C$ is inversely related to the water-use efficiency, defined as A/T, and
615 when P was low all models simulated an increase in water-use efficiency (Figure 7b). The Gain-
616 Risk model had the lowest water-use efficiency under unstressed conditions, likely due to the
617 lack of constraints on T when the hydraulic risk is low. This is consistent with the overestimation
618 of T during unstressed conditions seen in previous results. Models clearly simulate distinct
619 relationships between these measures of water-use efficiency and P during periods of both low
620 and high environmental stress.

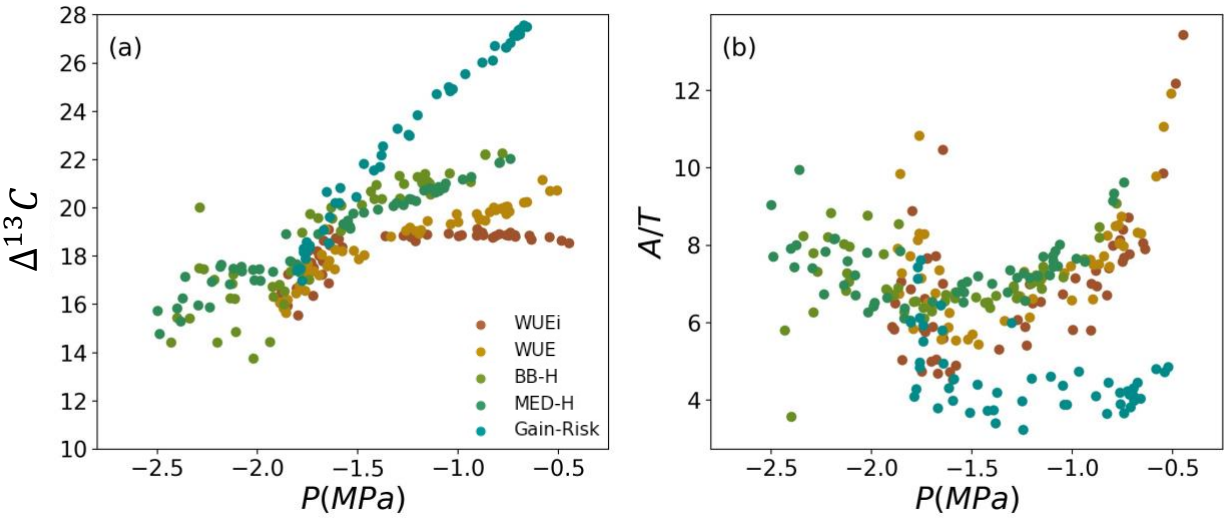

621
622 **Figure 7.** Simulated relationships between monthly mean daytime canopy water potential, P, and
623 $\Delta^{13}C$ (a) or assimilation/transpiration (A/T) (b) simulated for June, July, and August 2006–2018.

624

625 *3.5 Variability in information flows from VPD and SWP to T*

626

The influence of VPD and SWP together on T was measured by their multi-variate mutual information partitioned into redundant, synergistic, and unique information components. When water stress was low (SWP>75th percentile) the information from SWP and VPD together reduced 43% of uncertainty (entropy) in daily T (Figure 8). The remaining information about T can be attributed to the influence of the other environmental factors such as net radiation, which is a strong control on T in the spring when soil water is most available. The unique information from VPD reduced 23% of the uncertainty whereas the unique information from SWP and synergistic information reduced 8 and 10% of the uncertainty, respectively. This indicates that when water stress was low, VPD was a more influential control on T than SWP. When soil water stress was high (SWP<25th percentile) the observed SWP and VPD reduced 57% of uncertainty in T (Figure 8). In the water-stressed late summer months, photosynthetically active radiation and temperature are usually less limiting and thus VPD and SWP are more influential on T compared to the early spring months. The unique information from SWP and VPD reduced 17% and 15% of the uncertainty, respectively, and the synergistic information reduced an additional 23%. In both the cases, the redundant information between VPD and SWP was small.

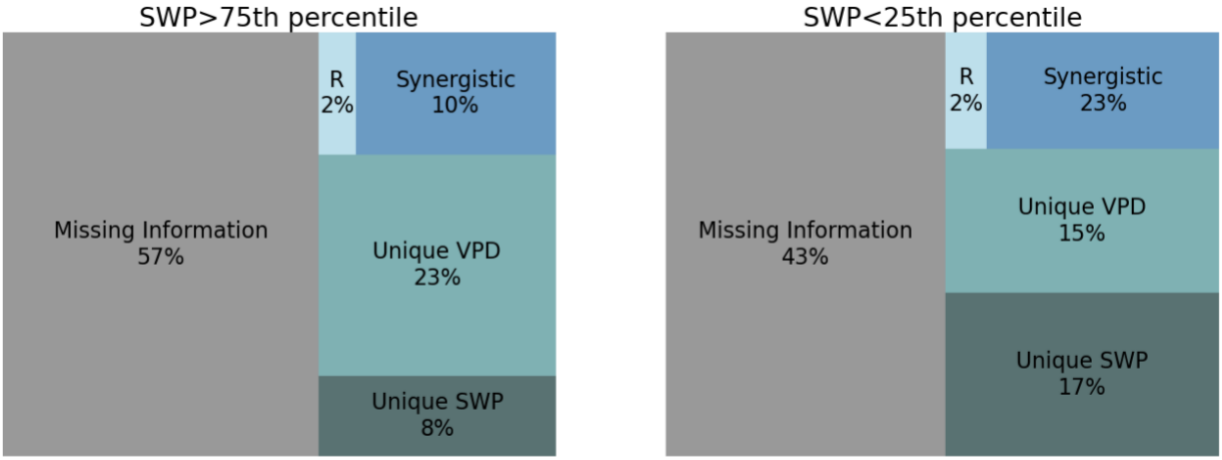

Figure 8. Reduction in uncertainty (mutual information) in daily transpiration rates attributable to vapor pressure deficit (VPD) and soil water potential (SWP), when SWP is above the 75th percentile (left) and below the 25th percentile (right). Mutual information is partitioned into synergistic, unique to VPD, unique to SWP, and redundant (R) information. The total area represents the entropy of transpiration and percentages are computed as the fraction of

649 transpiration entropy. Missing information represents the fraction of transpiration entropy that is
650 not shared with VPD and SWP.
651
652 We evaluated how well each model represented the functional relationships among daily VPD,
653 SWP and T by taking the difference between information flows calculated from measurements
654 and calculated from model simulations. When soil water stress was high (SWP<25th percentile)
655 the more mechanistic models (WUEi, WUE, Gain-Risk) had higher predictive performance
656 (lower A_p) than the semi-empirical models (BB-H, MED-H) and WUEi had the most accurate T
657 estimates (Figure 9a). The WUEi, WUE, and Gain-Risk models most accurately simulated the
658 total mutual information ($A_{f,t}$ closer to 0; Figure 9b) pointing to consistency in predictive and
659 functional performance. The BB-H and MED-H models most underestimated the total mutual
660 information contained in SWP and VPD about T and the Gain-Risk model was the only overly
661 deterministic model (positive $A_{f,t}$). In terms of the overall performance of information
662 partitioning WUE and MED-H were the most accurate ($A_{f,p}$ close to 0) (Figure 9c), despite not
663 having highest predictive performance. The Gain-Risk model had the poorest partitioning
664 accuracy (highest $A_{f,p}$), indicating that it may be reproducing the variability in T accurately but at
665 the expense of poorer representation of the individual information flows. All models (excluding
666 BB-H) accurately represented the unique information from SWP (Figure 9d) but the WUEi and
667 Gain-Risk models overestimated the unique information from VPD (Figure 9e). The BB-H
668 model overrepresented the synergistic information whereas the Gain-Risk model underestimated
669 the synergistic information (Figure 9f). All models accurately captured the redundant
670 information (Figure 9g).
671

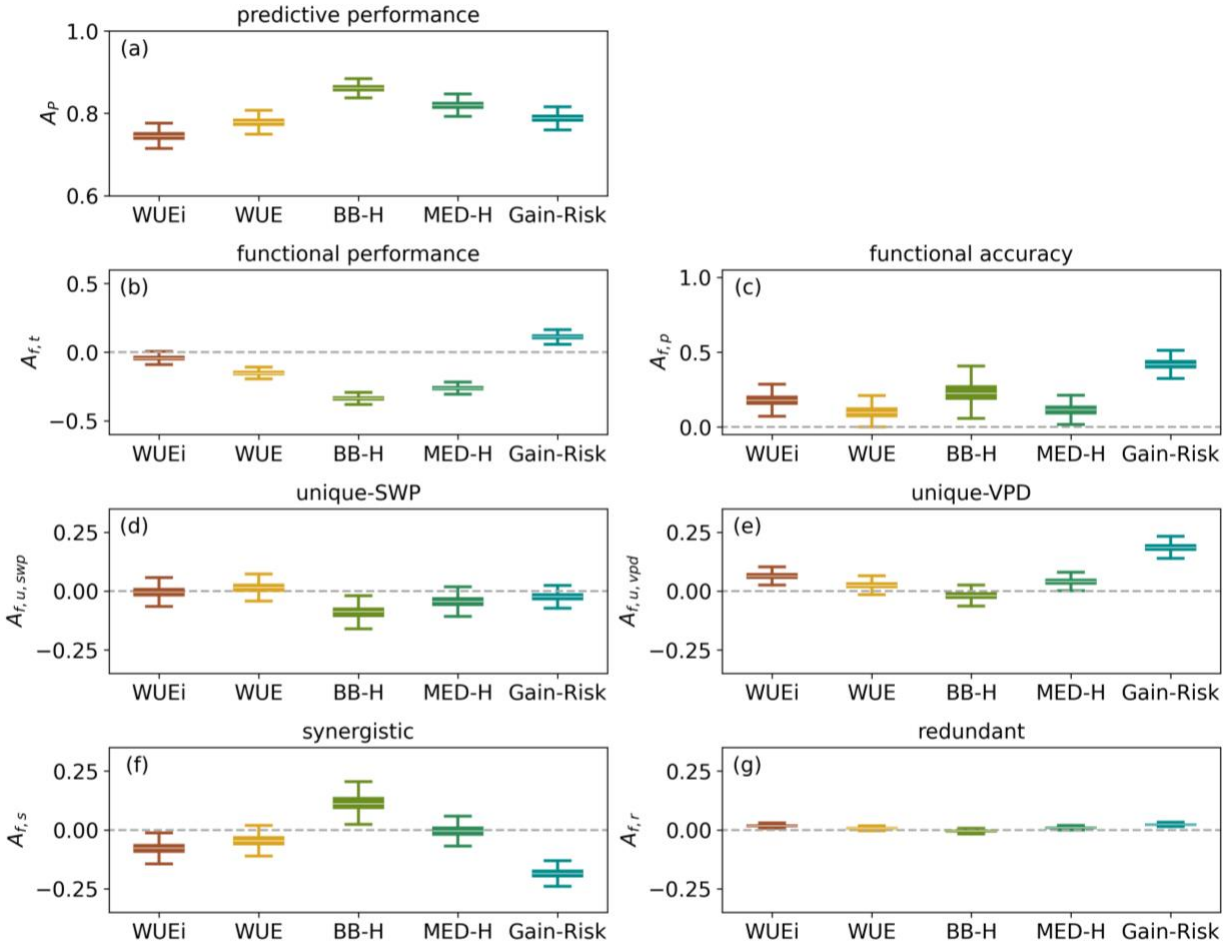

Figure 9. Evaluation of model performance of daily transpiration (T) during growing season (May-August) of 2006 through 2018 when soil water potential (SWP) was below the 25th percentile (high soil water stress). (a) Predictive performance (A_P, bits bit^{-1}) quantifies the relative fraction of information missing in the model about T compared to observations. (b) Total functional performance ($A_{f,T}$, bits bit^{-1}) quantifies the relative difference between observed and modeled total multi-variate mutual information from SWP and VPD about T. (c) Functional accuracy ($A_{f,P} = |A_{f,swp}| + |A_{f,VPD}| + |A_{f,S}| + |A_{f,R}|$, bits bit^{-1}) quantifies the relative difference between observed and modeled mutual information partitioning from SWP and VPD about T. The components of functional accuracy are partitioned into (d) unique from soil water potential ($A_{f,swp}$, bits bit^{-1}), (e) unique from VPD ($A_{f,VPD}$, bits bit^{-1}), (f) synergistic ($A_{f,S}$, bits bit^{-1}), and (g) redundant ($A_{f,R}$, bits bit^{-1}) information. Boxes represent the interquartile range of bootstrapped samples; whiskers represent 5th and 95th percentiles; and white lines represent medians. For all metrics a value of zero indicates a perfect model-data match.

When water is not limiting (SWP>75th percentile) the predictive performance of all models was indistinguishable (Figure S6). The BB-H had the best total functional performance; all other models overestimated the strength of the total multi-variate mutual information from SWP and VPD about T. The functional accuracy of the BB-H model outperformed all other models since all other models overestimate the functional control of VPD on T and underestimate the synergistic information.

4 Discussion

4.1 Representing plant hydraulic strategies

Plant water and carbon relations are strongly tied to the ways plants respond to hydrologic stress. It's common to generalize plant hydraulic strategies along a continuum between isohydric and anisohydric behavior. Although this framework is oversimplistic it can be useful (Kannenberg et al., 2021) when comparing behavior with common environmental forcings such as in this study. The hydraulic limitation imposed in this study in the BB-H and MED-H models represents more anisohydric behavior, as the model structure allows the canopy water potential to reach low mid-day levels (Figure 2). At low canopy water potentials, the BB-H and MED-H models increase the water-use efficiency (Figure 7) and constrain transpiration to peak in the morning (Figure 2 & 3). Given the functional form of the hydraulic limitation we impose, alternate parameterizations cannot sufficiently represent the isohydric behavior characteristic of ponderosa pines. A steeper hydraulic vulnerability constraint (achieved by modifying the b and c parameters in eq. 6) would prevent the canopy water potential from reaching very low values but only by modifying the g_1 parameter and thus reducing assimilation to near zero.

The structure of the WUEi and WUE models fundamentally represents isohydric water-use strategies (Fisher et al., 2006). The minimum leaf water potential threshold limits stomatal conductance at a prescribed canopy water potential which results in conservative water use. The WUEi and WUE models maintain relatively constant transpiration and canopy water potential throughout the day (Figure 2). Less conservative water-use behavior can be achieved by setting

the minimum leaf water potential parameter to very low values (e.g., -6 MPa), then the stomatal efficiency parameter constrains plant water-use. However, there is a trade-off; the low settings of stomatal efficiency required to achieve anisohydric behavior also limit carbon assimilation. Williams et al., (1996) applied the WUEi model to a mixed deciduous broadleaf stand and was able to capture anisohydric behavior early in the growing season when canopy water potentials remained above the *minLWP* (set to -2.5MPa) but in the late growing season when canopy water potentials were low the model constrained mid-day water-use and was unable to capture the observed anisohydric behavior.

The Gain-Risk model constrains the canopy water potential to avoid hydraulic damage. With the parameterization used in this application the model demonstrates conservative water use, maintaining relatively constant mid-day canopy water potentials (Figure 2). The Gain-Risk model can be parameterized to relax constraints on canopy water potential and can capture a range of water-use strategies as demonstrated by Sabot et al., (2020). However, the parameterization used here does not adequately capture the timing of water-use throughout the day (Figure 3). Ponderosa pines maximize canopy conductance and use water early in the day before the VPD gets too high (Figures 2 & 3), thus avoiding water loss while still maximizing carbon gain. The Gain-Risk model captures the early morning peak in canopy conductance (Figure 2), but it simulates transpiration peaking in the late afternoon, even under drought stress when the hydraulic risk is high. It is possible that alternate plant trait combinations would alter the diurnal cycle of transpiration. In addition, transpiration in the Gain-Risk model is very sensitive to soil water potential (see Figure 6 in Venturas et al., 2018) and any error in the diurnal cycle of soil or rhizosphere water potential propagates to transpiration. Future work is needed to determine if the Gain-Risk model can capture conservative water-use strategies on sub-daily temporal scales.

4.2 Canopy temperature

Accurately modeling canopy temperatures is critical for representing ecological processes, particularly as heat waves become more frequent and severe under changing climate conditions. While the biophysical drivers of canopy temperature vary among ecosystems, canopy

748 temperature is often more relevant to biological functioning than air temperature (Still et al.,
749 2019). The observed canopy temperature diverged from the air temperature by several degrees at
750 this site. At night, canopy temperatures cooled below air temperatures and during the day canopy
751 temperatures were nearly 3°C warmer than air temperatures (Figure 4). Similar behavior was
752 shown by Kim et al., (2016) who found canopy temperature to be a strong predictor of net
753 ecosystem exchange.
754
755 All models examined in this study were unable to capture the divergence of canopy temperature
756 from air temperature (Figure 4). Other modeling studies have found similar model deficiencies,
757 for example, Holm et al., (2014) found that the CLM4 was unable to reproduce the range of leaf
758 temperatures observed at a tropical site. Duursma and Medlyn, (2012) found that the MAESPA
759 model was unable to capture the vertical profile of canopy temperatures using a multilayer
760 canopy model. Venturas et al., (2018) compared leaf temperatures of Aspen measured with
761 thermocouples to leaf temperatures simulated with the Gain-Risk model and found the model
762 underestimated midday leaf temperatures (mean absolute leaf temperature error of 1.7°C or
763 5.2%). Biases in leaf temperature influence the calculation of leaf-to-air VPD (used in the
764 calculation of transpiration) and can propagate through photosynthetic and stomatal optimization
765 functions. Furthermore, since leaf metabolic processes depend non-linearly on leaf temperature
766 small biases can manifest into large discrepancies, impacting model performance. When the leaf
767 temperature was prescribed in the MED-H model using the observed canopy temperature, the
768 cumulative growing season mean transpiration was 5% higher. The increased morning
769 transpiration and decreased afternoon transpiration better matched the observed diurnal pattern
770 of sapflow measurements (Figure 5).
771
772 These findings emphasize the need to address model deficiencies in the representation of canopy
773 temperature. Big-leaf models have deficiencies in capturing canopy temperatures since the whole
774 canopy experiences equivalent air temperatures. Multilayer canopy models can capture the
775 vertical profiles of radiation and within-canopy air temperatures which studies have found to
776 improve simulated surface fluxes (Chen et al., 2016; Bonan et al., 2018). In the SPA multilayer
777 canopy model, the above-canopy temperature is applied at all canopy layers, assuming within-
778 canopy air is well-mixed. Bonan et al., (2021) demonstrated that using uniform vertical profiles

779 of air temperatures in multilayer canopy models results in nearly identical fluxes as big-leaf
780 models. When the well-mixed assumption is removed and the vertical profile of air temperatures
781 are resolved, Bonan et al., (2021) showed considerable improvement in canopy fluxes. This
782 suggests that a first step toward addressing canopy temperature biases in multilayer models
783 would be to resolve vertical air temperature profiles. A second step would be to examine the role
784 of leaf boundary layer processes, which also likely contribute to leaf temperature biases. Finally,
785 the accuracy of the radiation transfer scheme should be assessed, which requires within canopy
786 observational data.
787
788 *4.3 Water-use efficiency*
789
790 Stable carbon isotopes have long been used to provide information on plant water use efficiency
791 (Farquhar & Richards 1984; Farquhar et al., 1989; Condon, Richards & Farquhar 1993). The
792 dynamics of isotopic discrimination can be used to evaluate how ecosystem models respond to
793 environmental drivers on interannual timescales (Lavergne et al., 2019; 2020a; 2020b). Here we
794 illustrated the value of $\Delta^{13}C$ observations for discerning model behavior. The Gain-Risk model
795 simulates the strongest reduction in monthly mean $\Delta^{13}C$ in response to reduced canopy water
796 potential (Figure 7). This is because the Gain-Risk model varies the water use efficiency
797 optimally to maximize carbon gain while avoiding loss of hydraulic function. The WUEi model
798 maintains near constant $\Delta^{13}C$ until the minimum canopy water potential (-2 MPa) is reached. The
799 stomatal efficiency parameter defines the marginal water cost of carbon that constrains the
800 intrinsic water use efficiency ($\Delta A/\Delta g_s$) and thus the $\Delta^{13}C$. In the WUE model the stomatal
801 efficiency parameter defines the instantaneous water use efficiency ($\Delta A/\Delta T$) and thus modifies
802 the water use efficiency in response to VPD. Therefore, the decline in $\Delta^{13}C$ with reduced canopy
803 water potential simulated by the WUE model is likely attributable to the correlation between
804 VPD and canopy water potential.
805
806 The BB-H and MED-H models originally used a fixed water-use efficiency, defined by the g_1
807 parameter. Here we implemented a hydraulic stress constraint which modifies the g_1 parameter in
808 response to canopy water potential (eq. 5). The result is a linear reduction in $\Delta^{13}C$ with reduced
809 canopy water potential (Figure 7). Kennedy et al., (2019) implemented a similar constraint in the

CLM5 model but applied the hydraulic limitation by modifying Vcmax. Whether drought stress affects the water-use efficiency of plants or acts directly on photosynthetic capacity is still an open question. Zhou et al., (2013) found that downregulation of the g_1 parameter was insufficient to account for observed changes in GPP in response to water limitation, and thus modification of Vcmax was required. However, Lin et al., (2018) suggest that the g_1 parameter is not sensitive to water limitations and only the intercept, g_0, and GPP are sensitive to soil water availability.

Observations of $\Delta^{13}C$ would be a valuable tool for better understanding the effects of drought stress on plant gas exchange and may elucidate differences in model representations of hydraulic functioning. The National Ecological Observatory Network (NEON) measures atmospheric CO_2 isotope ratios across ecosystems at high temporal frequencies (Fiorella et al., 2021). We suggest that this observational network could serve as a valuable model testbed and encourage future cross-site model evaluation studies.

4.4 Information flows

We took an information theoretical approach to decompose multi-variate mutual information between transpiration and its key drivers to assess process representation in models independently of parametric assumptions. Similarly to Bassiouni & Vico, (2021), we found that all models had high overall functional performance (Figure 9). Generally, the more empirical models (BB-H & MED-H) had better functional performance when soil water was not limiting (Figure S6) while models with more mechanistic representations of hydraulic functioning (WUEi, WUE, Gain-Risk) had better functional performance when soil water availability was low (Figure 9). It is common for more empirical, multiplicative models (such as MED-H) to better represent synergistic information while more mechanistic additive models (such as Gain-Risk) can underestimate interactions among processes and thus trade synergistic for unique information. This result illustrates how semi-empirical models can compensate for incomplete process representation and capture functional relationships across scales, while incomplete processes in more mechanistic models are more easily discernible. The WUEi and Gain-Risk models had larger tradeoffs between predictive performance and functional accuracy compared to WUE and MED-H, pointing to the possibility that the WUEi and Gain-Risk models accurately

estimate the variability in transpiration at the expense of poorer process representations. This finding was clearer from the information metrics than the individual processes diagnostics.

This study builds upon the work of Bassiouni & Vico, (2021) by implementing stomatal models within multi-layer canopy (and big-leaf) ecosystem models and solving optimization routines numerically. The findings of both studies agree; more mechanistic representations of plant hydraulic functioning did not substantially improve predictive performance or functional accuracy. Our results indicate that semi-empirical models, in particular MED-H, can be effectively adapted to incorporate hydraulic constraints based on measurable plant traits. Model evaluation metrics based on information flows allowed us to go beyond evaluating model performance based on magnitude and seasonality (e.g. Sabot et al., 2020) and examine the causal relationships among the physiological controls on transpiration. The performance metrics also complement the analysis of individual model sensitivities of G_c to VPD and C_i/C_a to P because they help differentiate between effective functional differences and predictive accuracy. However, additional analyses are needed to further interpret the mechanisms driving information-based performance metrics and test whether models with improved functional accuracy perform better under non-stationary climate conditions. We encourage cross-scale model evaluations spanning a range of ecosystems and advocate for the use of information theory to evaluate causal relationships in complex ecological systems.

5 Conclusions

As the consequences of model representation of stomatal functioning become apparent at large scales (e.g., Kala et al., 2016), much effort has gone into updating the representation of hydraulic functioning in Earth System Models (e.g. Kennedy et al., 2019, Eller et al., 2020, Sabot et al., 2020). To ensure processes are adequately captured across scales, model evaluations must go beyond mean state and variability of leaf-level gas exchange measurements and find new ways to diagnose functional performance and leverage new analytical techniques. Here, we compared a suite of ecosystem models with different representations of hydraulic constraints on stomatal function and identified model specific strengths and deficiencies at a semi-arid ponderosa pine site. We found that models generally performed similarly under unstressed conditions, but

performance diverged under atmospheric and soil drought. The more empirical models over estimated synergistic information flows between soil water potential and vapor pressure deficit to transpiration, while the more mechanistic models were overly deterministic.

This analysis highlights three directions for future ecosystem model development and evaluation: First, it's likely that model structure constrains the flexibility of models to represent a broad spectrum of (an)isohydric behavior. Second, both multilayer canopy and big-leaf models were unable to capture the magnitude of the divergence of canopy temperature from air temperature and given the crucial role of canopy temperature in simulating metabolic processes, diagnosing the causes of model biases should be a priority. Lastly, models diverged in their representation of $\Delta^{13}C$ under stress thus measurements of stable carbon isotopes may help characterize ecosystem function and elucidate differences attributable to model structure. Future work is needed to explore model structural constraints on ecosystem functional behavior.

Acknowledgments

The authors would like to thank Matt Williams and Luke Smallman for technical support for the SPA model, and Henry Todd for technical support with the Gain-Risk model. This work was funded by the National Science Foundation, Division of Environmental Biology, through the macrosystems biology and NEON-enable science program grant number DEB-1802885. MB received funding from the European Commission and Swedish Research Council for Sustainable Development (FORMAS) (grant 2018-02787) in the frame of the international consortium iAqueduct financed under the 2018 Joint call of the WaterWorks2017 ERA-NET Cofund. MDV was supported by H2020-MSCA-IF-2019 grant No. 882216.

Open research

Model code, configuration, and simulations, observational data, and PYTHON scripts required to reproduce this analysis are openly available at https://zenodo.org/badge/latestdoi/430187802

References

900 Anderegg, W. R. L., Wolf, A., Arango-Velez, A., Choat, B., Chmura, D. J., Jansen, S., Kolb, T.,
901 Li, S., Meinzer, F. C., Pita, P., Resco de Dios, V., Sperry, J. S., Wolfe, B. T., & Pacala, S.
902 (2018). Woody plants optimise stomatal behaviour relative to hydraulic risk. *Ecology*
903 *Letters*, *21*(7), 968–977. https://doi.org/10.1111/ele.12962
904 Aphalo, P. J., & Jarvis, P. G. (1991). Do stomata respond to relative humidity? *Plant, Cell &*
905 *Environment*, *14*(1), 127–132. https://doi.org/10.1111/j.1365-3040.1991.tb01379.x
906 Ball, J. T., Woodrow, I. E., & Berry, J. A. (1987). A Model Predicting Stomatal Conductance
907 and its Contribution to the Control of Photosynthesis under Different Environmental
908 Conditions. In J. Biggins (Ed.), *Progress in Photosynthesis Research: Volume 4*
909 *Proceedings of the VIIth International Congress on Photosynthesis Providence, Rhode*
910 *Island, USA, August 10–15, 1986* (pp. 221–224). Springer Netherlands.
911 https://doi.org/10.1007/978-94-017-0519-6_48
912 Bassiouni, M., & Vico, G. (2021). Parsimony vs predictive and functional performance of three
913 stomatal optimization principles in a big-leaf framework. *New Phytologist*, *231*(2), 586–
914 600. https://doi.org/10.1111/nph.17392
915 Bonan, G. B. (1995). Land-atmosphere CO2 exchange simulated by a land surface process
916 model coupled to an atmospheric general circulation model. *Journal of Geophysical*
917 *Research: Atmospheres*, *100*(D2), 2817–2831. https://doi.org/10.1029/94JD02961
918 Bonan, G. B., Patton, E. G., Finnigan, J. J., Baldocchi, D. D., & Harman, I. N. (2021). Moving
919 beyond the incorrect but useful paradigm: Reevaluating big-leaf and multilayer plant
920 canopies to model biosphere-atmosphere fluxes – a review. *Agricultural and Forest*
921 *Meteorology*, *306*, 108435. https://doi.org/10.1016/j.agrformet.2021.108435
922 Bonan, G. B., Patton, E. G., Harman, I. N., Oleson, K. W., Finnigan, J. J., Lu, Y., & Burakowski,
923 E. A. (2018). Modeling canopy-induced turbulence in the Earth system: A unified
924 parameterization of turbulent exchange within plant canopies and the roughness sublayer
925 (CLM-ml v0). *Geoscientific Model Development*, *11*(4), 1467–1496.
926 https://doi.org/10.5194/gmd-11-1467-2018
927 Bonan, G. B., Williams, M., Fisher, R. A., & Oleson, K. W. (2014). Modeling stomatal
928 conductance in the earth system: Linking leaf water-use efficiency and water transport
929 along the soil–plant–atmosphere continuum. *Geoscientific Model Development*, *7*(5),
930 2193–2222. https://doi.org/10.5194/gmd-7-2193-2014

931 Bowling, D. R., McDowell, N. G., Bond, B. J., Law, B. E., & Ehleringer, J. R. (2002). ^{13}C
932 content of ecosystem respiration is linked to precipitation and vapor pressure deficit.
933 *Oecologia*, *131*(1), 113–124. https://doi.org/10.1007/s00442-001-0851-y
934 Buckley, T. N. (2005). The control of stomata by water balance. *New Phytologist*, *168*(2), 275–
935 292. https://doi.org/10.1111/j.1469-8137.2005.01543.x
936 Buckley, T. N. (2017). Modeling Stomatal Conductance. *Plant Physiology*, *174*(2), 572–582.
937 https://doi.org/10.1104/pp.16.01772
938 Buckley, T. N. (2019). How do stomata respond to water status? *New Phytologist*, *224*(1), 21–
939 36. https://doi.org/10.1111/nph.15899
940 Fiorella, R. P., Good, S. P., Allen, S. T., Guo, J. S., Still, C. J., Noone, D. C., Anderegg, W.R.,
941 Florian, C.R., Luo, H., Pingintha-Durden, N. & Bowen, G. J. (2021). Calibration
942 Strategies for Detecting Macroscale Patterns in NEON Atmospheric Carbon Isotope
943 Observations. *Journal of Geophysical Research: Biogeosciences*, *126*(3),
944 e2020JG005862.
945 Chen, Y., Ryder, J., Bastrikov, V., McGrath, M. J., Naudts, K., Otto, J., Ottlé, C., Peylin, P.,
946 Polcher, J., Valade, A., Black, A., Elbers, J. A., Moors, E., Foken, T., van Gorsel, E.,
947 Haverd, V., Heinesch, B., Tiedemann, F., Knohl, A., … Luyssaert, S. (2016). Evaluating
948 the performance of land surface model ORCHIDEE-CAN v1.0 on water and energy flux
949 estimation with a single- and multi-layer energy budget scheme. *Geoscientific Model*
950 *Development*, *9*(9), 2951–2972. https://doi.org/10.5194/gmd-9-2951-2016
951 Condon, A. G., Richards, R. A., & Farquhar, G. D. (1993). Relationships between carbon isotope
952 discrimination, water use efficiency and transpiration efficiency for dryland wheat.
953 *Australian Journal of Agricultural Research*, *44*(8), 1693–1711.
954 https://doi.org/10.1071/ar9931693
955 Cover T.M., & Thomas J. A., (2012). Elements of information theory. New York, NY, USA:
956 John Wiley & Sons.
957 Cowan, I. R., & Farquhar, G. D. (1977). Stomatal function in relation to leaf metabolism and
958 environment. *Integration of Activity in the Higher Plant*, Cambridge University Press,
959 Cambridge, 471–505. https://pubmed.ncbi.nlm.nih.gov/756635/

960 Cox, P. M., Huntingford, C., & Harding, R. J. (1998). A canopy conductance and photosynthesis
961 model for use in a GCM land surface scheme. *Journal of Hydrology*, *212–213*, 79–94.
962 https://doi.org/10.1016/S0022-1694(98)00203-0
963 Damour, G., Simonneau, T., Cochard, H., & Urban, L. (2010). An overview of models of
964 stomatal conductance at the leaf level. *Plant, Cell & Environment*, *33*(9), 1419–1438.
965 https://doi.org/10.1111/j.1365-3040.2010.02181.x
966 Domec, J.-C., Warren, J. M., Meinzer, F. C., Brooks, J. R., & Coulombe, R. (2004). Native root
967 xylem embolism and stomatal closure in stands of Douglas-fir and ponderosa pine:
968 Mitigation by hydraulic redistribution. *Oecologia*, *141*(1), 7–16.
969 https://doi.org/10.1007/s00442-004-1621-4
970 Duursma, R. A., & Medlyn, B. E. (2012). MAESPA: A model to study interactions between
971 water limitation, environmental drivers and vegetation function at tree and stand levels,
972 with an example application to [CO_2] × drought interactions. *Geoscientific Model*
973 *Development*, *5*(4), 919–940. https://doi.org/10.5194/gmd-5-919-2012
974 Eller, C. B., Rowland, L., Mencuccini, M., Rosas, T., Williams, K., Harper, A., Medlyn, B. E.,
975 Wagner, Y., Klein, T., Teodoro, G. S., Oliveira, R. S., Matos, I. S., Rosado, B. H. P.,
976 Fuchs, K., Wohlfahrt, G., Montagnani, L., Meir, P., Sitch, S., & Cox, P. M. (2020).
977 Stomatal optimization based on xylem hydraulics (SOX) improves land surface model
978 simulation of vegetation responses to climate. *New Phytologist*, *226*(6), 1622–1637.
979 https://doi.org/10.1111/nph.16419
980 Evans, J. R., & Von Caemmerer, S. (2013). Temperature response of carbon isotope
981 discrimination and mesophyll conductance in tobacco. *Plant, Cell & Environment*, *36*(4),
982 745–756. https://doi.org/10.1111/j.1365-3040.2012.02591.x
983 Farquhar, G. D., von Caemmerer, S., & Berry, J. A. (1980). A biochemical model of
984 photosynthetic CO_2 assimilation in leaves of C3 species. *Planta*, 149, 78–90.
985 Farquhar, G. D., O'Leary, M. H., & Berry, J. A. (1982). On the Relationship Between Carbon
986 Isotope Discrimination and the Intercellular Carbon Dioxide Concentration in Leaves.
987 *Functional Plant Biology*, *9*(2), 121–137. https://doi.org/10.1071/pp9820121
988 Farquhar, G. D., & von Caemmerer, S. (1982). Modelling of Photosynthetic Response to
989 Environmental Conditions. In O. L. Lange, P. S. Nobel, C. B. Osmond, & H. Ziegler

(Eds.), *Physiological Plant Ecology II: Water Relations and Carbon Assimilation* (pp. 549–587). Springer. https://doi.org/10.1007/978-3-642-68150-9_17

Farquhar, G. D., & Richards, R. A. (1984). Isotopic Composition of Plant Carbon Correlates With Water-Use Efficiency of Wheat Genotypes. *Functional Plant Biology*, *11*(6), 539–552. https://doi.org/10.1071/pp9840539

Farquhar, G. D., Ehleringer, J. R., & Hubick, K. T. (1989) Carbon isotope discrimination and photosynthesis. Annual Review Plant Physiology Plant Molecular Biology *40*, 503–537.

Feng, X. (1999). Trends in intrinsic water-use efficiency of natural trees for the past 100–200 years: a response to atmospheric CO2 concentration. *Geochimica et Cosmochimica Acta*, *63*(13-14), 1891-1903.

Fiorella, R. P., Good, S. P., Allen, S. T., Guo, J. S., Still, C. J., Noone, D. C., Anderegg, W. R. L., Florian, C. R., Luo, H., Pingintha-Durden, N., & Bowen, G. J. (2021). Calibration Strategies for Detecting Macroscale Patterns in NEON Atmospheric Carbon Isotope Observations. *Journal of Geophysical Research: Biogeosciences*, *126*(3), e2020JG005862. https://doi.org/10.1029/2020JG005862

Fisher, R. A., Williams, M., Do Vale, R. L., Da Costa, A. L., & Meir, P. (2006). Evidence from Amazonian forests is consistent with isohydric control of leaf water potential. *Plant, Cell & Environment*, *29*(2), 151–165. https://doi.org/10.1111/j.1365-3040.2005.01407.x

Franks, P. J., Berry, J. A., Lombardozzi, D. L., & Bonan, G. B. (2017). Stomatal Function across Temporal and Spatial Scales: Deep-Time Trends, Land-Atmosphere Coupling and Global Models. *Plant Physiology*, *174*(2), 583–602. https://doi.org/10.1104/pp.17.00287

Goodwell, A. E., Jiang, P., Ruddell, B. L., & Kumar, P. (2020). Debates—Does Information Theory Provide a New Paradigm for Earth Science? Causality, Interaction, and Feedback. *Water Resources Research*, *56*(2), e2019WR024940. https://doi.org/10.1029/2019WR024940

Goodwell, A. E., & Kumar, P. (2017). Temporal information partitioning: Characterizing synergy, uniqueness, and redundancy in interacting environmental variables. *Water Resources Research*, *53*(7), 5920–5942. https://doi.org/10.1002/2016WR020216

Granier, A. (1987). Evaluation of transpiration in a Douglas-fir stand by means of sap flow measurements. *Tree Physiology*, *3*(4), 309–320. https://doi.org/10.1093/treephys/3.4.309

1020 Hill, T. C., Williams, M., & Moncrieff, J. B. (2008). Modeling feedbacks between a boreal forest
1021 and the planetary boundary layer. *Journal of Geophysical Research: Atmospheres*,
1022 *113*(D15). https://doi.org/10.1029/2007JD009412
1023 Holm, J. A., Jardine, K., Guenther, A. B., Chambers, J. Q., & Tribuzy, E. (2014). Evaluation of
1024 MEGAN-CLM parameter sensitivity to predictions of isoprene emissions from an
1025 Amazonian rainforest. *Atmospheric Chemistry and Physics Discussions*, *14*(17), 23995–
1026 24041. https://doi.org/10.5194/acpd-14-23995-2014
1027 Irvine, J., Law, B. E., Kurpius, M. R., Anthoni, P. M., Moore, D., & Schwarz, P. A. (2004). Age-
1028 related changes in ecosystem structure and function and effects on water and carbon
1029 exchange in ponderosa pine. *Tree Physiology*, *24*(7), 753–763.
1030 https://doi.org/10.1093/treephys/24.7.753
1031 Irvine, J., Law, B. E., Martin, J. G., & Vickers, D. (2008). Interannual variation in soil CO2
1032 efflux and the response of root respiration to climate and canopy gas exchange in mature
1033 ponderosa pine. *Global Change Biology*, *14*(12), 2848–2859.
1034 https://doi.org/10.1111/j.1365-2486.2008.01682.x
1035 Johnson, D. M., Woodruff, D. R., McCulloh, K. A., & Meinzer, F. C. (2009). Leaf hydraulic
1036 conductance, measured in situ, declines and recovers daily: Leaf hydraulics, water
1037 potential and stomatal conductance in four temperate and three tropical tree species. *Tree*
1038 *Physiology*, *29*(7), 879–887. https://doi.org/10.1093/treephys/tpp031
1039 Jones, H. G., & Jones, H. G. (1992). *Plants and Microclimate: A Quantitative Approach to*
1040 *Environmental Plant Physiology*. Cambridge University Press.
1041 Kala, J., De Kauwe, M. G., Pitman, A. J., Medlyn, B. E., Wang, Y.-P., Lorenz, R., & Perkins-
1042 Kirkpatrick, S. E. (2016). Impact of the representation of stomatal conductance on model
1043 projections of heatwave intensity. *Scientific Reports*, *6*(1), 23418.
1044 https://doi.org/10.1038/srep23418
1045 Kannenberg, S. A., Guo, J. S., Novick, K. A., Anderegg, W. R. L., Feng, X., Kennedy, D.,
1046 Konings, A. G., Martínez-Vilalta, J., & Matheny, A. M. (2021). Opportunities, challenges
1047 and pitfalls in characterizing plant water-use strategies. *Functional Ecology*, *n/a*(n/a).
1048 https://doi.org/10.1111/1365-2435.13945
1049 Kennedy, D., Swenson, S., Oleson, K. W., Lawrence, D. M., Fisher, R., Costa, A. C. L. da, &
1050 Gentine, P. (2019). Implementing Plant Hydraulics in the Community Land Model,

Version 5. *Journal of Advances in Modeling Earth Systems*, *11*(2), 485–513. https://doi.org/10.1029/2018MS001500

Kim, Y., Still, C. J., Hanson, C. V., Kwon, H., Greer, B. T., & Law, B. E. (2016). Canopy skin temperature variations in relation to climate, soil temperature, and carbon flux at a ponderosa pine forest in central Oregon. *Agricultural and Forest Meteorology*, *226–227*, 161–173. https://doi.org/10.1016/j.agrformet.2016.06.001

Koepke, D. F., & Kolb, T. E. (2013). Species Variation in Water Relations and Xylem Vulnerability to Cavitation at a Forest-Woodland Ecotone. *Forest Science*, *59*(5), 524–535. https://doi.org/10.5849/forsci.12-053

Kwon, H., Law, B. E., Thomas, C. K., & Johnson, B. G. (2018). The influence of hydrological variability on inherent water use efficiency in forests of contrasting composition, age, and precipitation regimes in the Pacific Northwest. *Agricultural and Forest Meteorology*, *249*(C). https://doi.org/10.1016/j.agrformet.2017.08.006

Lavergne, A., Graven, H., De Kauwe, M. G., Keenan, T. F., Medlyn, B. E., & Prentice, I. C. (2019). Observed and modelled historical trends in the water-use efficiency of plants and ecosystems. *Global Change Biology*, *25*(7), 2242–2257. https://doi.org/10.1111/gcb.14634

Lavergne, A., Sandoval, D., Hare, V. J., Graven, H., & Prentice, I. C. (2020a). Impacts of soil water stress on the acclimated stomatal limitation of photosynthesis: Insights from stable carbon isotope data. *Global Change Biology*, *26*(12), 7158–7172. https://doi.org/10.1111/gcb.15364

Lavergne, A., Voelker, S., Csank, A., Graven, H., de Boer, H. J., Daux, V., Robertson, I., Dorado-Liñán, I., Martínez-Sancho, E., Battipaglia, G., Bloomfield, K. J., Still, C. J., Meinzer, F. C., Dawson, T. E., Julio Camarero, J., Clisby, R., Fang, Y., Menzel, A., Keen, R. M., … Prentice, I. C. (2020b). Historical changes in the stomatal limitation of photosynthesis: Empirical support for an optimality principle. *New Phytologist*, *225*(6), 2484–2497. https://doi.org/10.1111/nph.16314

Law, B. E., Cescatti, A., & Baldocchi, D. D. (2001). Leaf area distribution and radiative transfer in open-canopy forests: Implications for mass and energy exchange. *Tree Physiology*, *21*(12–13), 777–787. https://doi.org/10.1093/treephys/21.12-13.777

1081 Leuning, R. (1995). A critical appraisal of a combined stomatal-photosynthesis model for C3
1082 plants. *Plant, Cell & Environment*, *18*(4), 339-355.
1083 Li, B., & Good, S. P. (2021). Information-based uncertainty decomposition in dual-channel
1084 microwave remote sensing of soil moisture. *Hydrology and Earth System Sciences*, *25*(9),
1085 5029–5045. https://doi.org/10.5194/hess-25-5029-2021
1086 Lin, C., Gentine, P., Huang, Y., Guan, K., Kimm, H., & Zhou, S. (2018). Diel ecosystem
1087 conductance response to vapor pressure deficit is suboptimal and independent of soil
1088 moisture. *Agricultural and Forest Meteorology*, *250–251*, 24–34.
1089 https://doi.org/10.1016/j.agrformet.2017.12.078
1090 Lin, Y.-S., Medlyn, B. E., Duursma, R. A., Prentice, I. C., Wang, H., Baig, S., Eamus, D., de
1091 Dios, V. R., Mitchell, P., Ellsworth, D. S., de Beeck, M. O., Wallin, G., Uddling, J.,
1092 Tarvainen, L., Linderson, M.-L., Cernusak, L. A., Nippert, J. B., Ocheltree, T. W.,
1093 Tissue, D. T., … Wingate, L. (2015). Optimal stomatal behaviour around the world.
1094 *Nature Climate Change*, *5*(5), 459–464. https://doi.org/10.1038/nclimate2550
1095 Love, D. M., Venturas, M. D., Sperry, J. S., Brooks, P. D., Pettit, J. L., Wang, Y., Anderegg, W.
1096 R. L., Tai, X., & Mackay, D. S. (2019). Dependence of Aspen Stands on a Subsurface
1097 Water Subsidy: Implications for Climate Change Impacts. *Water Resources Research*,
1098 *55*(3), 1833–1848. https://doi.org/10.1029/2018WR023468
1099 McKay, M. D., Beckman, R. J., & Conover, W. J. (1979). A Comparison of Three Methods for
1100 Selecting Values of Input Variables in the Analysis of Output from a Computer Code.
1101 *Technometrics*, *21*(2), 239–245. https://doi.org/10.2307/1268522
1102 Medlyn, B. E., Duursma, R. A., Eamus, D., Ellsworth, D. S., Prentice, I. C., Barton, C. V. M.,
1103 Crous, K. Y., De Angelis, P., Freeman, M., & Wingate, L. (2011). Reconciling the
1104 optimal and empirical approaches to modelling stomatal conductance. *Global Change*
1105 *Biology*, *17*(6), 2134–2144. https://doi.org/10.1111/j.1365-2486.2010.02375.x
1106 Medlyn, B. E., De Kauwe, M. G., Zaehle, S., Walker, A. P., Duursma, R. A., Luus, K.,
1107 Mishurov, M., Pak, B., Smith, B., Wang, Y.-P., Yang, X., Crous, K. Y., Drake, J. E.,
1108 Gimeno, T. E., Macdonald, C. A., Norby, R. J., Power, S. A., Tjoelker, M. G., &
1109 Ellsworth, D. S. (2016). Using models to guide field experiments: A priori predictions for
1110 the CO2 response of a nutrient- and water-limited native Eucalypt woodland. *Global*
1111 *Change Biology*, *22*(8), 2834–2851. https://doi.org/10.1111/gcb.13268

1112 Meinzer, F. C., Johnson, D. M., Lachenbruch, B., McCulloh, K. A., & Woodruff, D. R. (2009).
1113 Xylem hydraulic safety margins in woody plants: Coordination of stomatal control of
1114 xylem tension with hydraulic capacitance. *Functional Ecology*, *23*(5), 922–930.
1115 https://doi.org/10.1111/j.1365-2435.2009.01577.x
1116 Mencuccini, M., Manzoni, S., & Christoffersen, B. (2019). Modelling water fluxes in plants:
1117 From tissues to biosphere. *New Phytologist*, *222*(3), 1207–1222.
1118 https://doi.org/10.1111/nph.15681
1119 Misson, L., Panek, J. A., & Goldstein, A. H. (2004). A comparison of three approaches to
1120 modeling leaf gas exchange in annually drought-stressed ponderosa pine forests. *Tree*
1121 *Physiology*, *24*(5), 529–541. https://doi.org/10.1093/treephys/24.5.529
1122 Monteith, J., & Unsworth, M. (1990). *Principles of environmental physics: plants, animals, and*
1123 *the atmosphere*. Academic Press.
1124 Novick, K. A., Ficklin, D. L., Stoy, P. C., Williams, C. A., Bohrer, G., Oishi, A. C., Papuga, S.
1125 A., Blanken, P. D., Noormets, A., Sulman, B. N., Scott, R. L., Wang, L., & Phillips, R. P.
1126 (2016). The increasing importance of atmospheric demand for ecosystem water and
1127 carbon fluxes. *Nature Climate Change*, *6*(11), 1023–1027.
1128 https://doi.org/10.1038/nclimate3114
1129 Powell, T. L., Galbraith, D. R., Christoffersen, B. O., Harper, A., Imbuzeiro, H. M. A., Rowland,
1130 L., Almeida, S., Brando, P. M., da Costa, A. C. L., Costa, M. H., Levine, N. M., Malhi,
1131 Y., Saleska, S. R., Sotta, E., Williams, M., Meir, P., & Moorcroft, P. R. (2013).
1132 Confronting model predictions of carbon fluxes with measurements of Amazon forests
1133 subjected to experimental drought. *New Phytologist*, *200*(2), 350–365.
1134 https://doi.org/10.1111/nph.12390
1135 Reinhardt, E., Scott, J., Gray, K., & Keane, R. (2006). Estimating canopy fuel characteristics in
1136 five conifer stands in the western United States using tree and stand measurements.
1137 *Canadian Journal of Forest Research*, *36*(11), 2803–2814. https://doi.org/10.1139/x06-
1138 157
1139 Ruddell, B. L., Drewry, D. T., & Nearing, G. S. (2019). Information Theory for Model
1140 Diagnostics: Structural Error is Indicated by Trade-Off Between Functional and
1141 Predictive Performance. *Water Resources Research*, *55*(8), 6534–6554.
1142 https://doi.org/10.1029/2018WR023692

1143 Ruddell, B. L., & Kumar, P. (2009). Ecohydrologic process networks: 1. Identification. *Water*
1144 *Resources Research*, *45*(3). https://doi.org/10.1029/2008WR007279
1145 Ruehr, N. K., Law, B. E., Quandt, D., & Williams, M. (2014). Effects of heat and drought on
1146 carbon and water dynamics in a regenerating semi-arid pine forest: A combined
1147 experimental and modeling approach. *Biogeosciences*, *11*(15), 4139–4156.
1148 https://doi.org/10.5194/bg-11-4139-2014
1149 Sabot, M. E. B., De Kauwe, M. G., Pitman, A. J., Medlyn, B. E., Verhoef, A., Ukkola, A. M., &
1150 Abramowitz, G. (2020). Plant profit maximization improves predictions of European
1151 forest responses to drought. *New Phytologist*, *226*(6), 1638–1655.
1152 https://doi.org/10.1111/nph.16376
1153 Saltelli, A., & Bolado, R. (1998). An alternative way to compute Fourier amplitude sensitivity
1154 test (FAST). *Computational Statistics & Data Analysis*, *26*(4), 445–460.
1155 https://doi.org/10.1016/S0167-9473(97)00043-1
1156 Saxton, K. E., Rawls, W. J., Romberger, J. S., & Papendick, R. I. (1986). Estimating Generalized
1157 Soil-water Characteristics from Texture. *Soil Science Society of America Journal*, *50*(4),
1158 1031–1036. https://doi.org/10.2136/sssaj1986.03615995005000040039x
1159 Schwarz, P. A., Law, B. E., Williams, M., Irvine, J., Kurpius, M., & Moore, D. (2004). Climatic
1160 versus biotic constraints on carbon and water fluxes in seasonally drought-affected
1161 ponderosa pine ecosystems. *Global Biogeochemical Cycles*, *18*(4).
1162 https://doi.org/10.1029/2004GB002234
1163 Shannon, C. E. (1948). A mathematical theory of communication. *The Bell System Technical*
1164 *Journal*, *27*(3), 379–423. https://doi.org/10.1002/j.1538-7305.1948.tb01338.x
1165 Smallman, T. L., Moncrieff, J. B., & Williams, M. (2013). WRFv3.2-SPAv2: Development and
1166 validation of a coupled ecosystem–atmosphere model, scaling from surface fluxes of CO_2
1167 and energy to atmospheric profiles. *Geoscientific Model Development*, *6*(4), 1079–1093.
1168 https://doi.org/10.5194/gmd-6-1079-2013
1169 Sperry, J. S., & Love, D. M. (2015). What plant hydraulics can tell us about responses to
1170 climate-change droughts. *New Phytologist*, *207*(1), 14–27.
1171 https://doi.org/10.1111/nph.13354
1172 Sperry, J. S., Venturas, M. D., Anderegg, W. R. L., Mencuccini, M., Mackay, D. S., Wang, Y., &
1173 Love, D. M. (2017). Predicting stomatal responses to the environment from the

optimization of photosynthetic gain and hydraulic cost. *Plant, Cell & Environment*, *40*(6), 816–830. https://doi.org/10.1111/pce.12852

Sperry, J. S., Venturas, M. D., Todd, H. N., Trugman, A. T., Anderegg, W. R. L., Wang, Y., & Tai, X. (2019). The impact of rising CO2 and acclimation on the response of US forests to global warming. *Proceedings of the National Academy of Sciences*, *116*(51), 25734–25744. https://doi.org/10.1073/pnas.1913072116

Sperry, J. S., Wang, Y., Wolfe, B. T., Mackay, D. S., Anderegg, W. R. L., McDowell, N. G., & Pockman, W. T. (2016). Pragmatic hydraulic theory predicts stomatal responses to climatic water deficits. *New Phytologist*, *212*(3), 577–589. https://doi.org/10.1111/nph.14059

Still, C., Powell, R., Aubrecht, D., Kim, Y., Helliker, B., Roberts, D., Richardson, A. D., & Goulden, M. (2019). Thermal imaging in plant and ecosystem ecology: Applications and challenges. *Ecosphere*, *10*(6), e02768. https://doi.org/10.1002/ecs2.2768

Stout, D. H., & Sala, A. (2003). Xylem vulnerability to cavitation in Pseudotsuga menziesii and Pinus ponderosa from contrasting habitats. *Tree Physiology*. https://doi.org/10.1093/TREEPHYS/23.1.43

Sus, O., Poyatos, R., Barba, J., Carvalhais, N., Llorens, P., Williams, M., & Vilalta, J. M. (2014). Time variable hydraulic parameters improve the performance of a mechanistic stand transpiration model. A case study of Mediterranean Scots pine sap flow data assimilation. *Agricultural and Forest Meteorology*, *198–199*, 168–180. https://doi.org/10.1016/j.agrformet.2014.08.009

Thomas, C. K., Law, B. E., Irvine, J., Martin, J. G., Pettijohn, J. C., & Davis, K. J. (2009). Seasonal hydrology explains interannual and seasonal variation in carbon and water exchange in a semiarid mature ponderosa pine forest in central Oregon. *Journal of Geophysical Research: Biogeosciences*, *114*(G4). https://doi.org/10.1029/2009JG001010

Tuzet, A., Perrier, A., & Leuning, R. (2003). A coupled model of stomatal conductance, photosynthesis and transpiration. *Plant, Cell & Environment*, *26*(7), 1097–1116. https://doi.org/10.1046/j.1365-3040.2003.01035.x

Ukkola, A. M., Kauwe, M. G. D., Pitman, A. J., Best, M. J., Abramowitz, G., Haverd, V., Decker, M., & Haughton, N. (2016). Land surface models systematically overestimate the intensity, duration and magnitude of seasonal-scale evaporative droughts.

Environmental Research Letters, *11*(10), 104012. https://doi.org/10.1088/1748-9326/11/10/104012

Ulrich, D. E. M., Still, C., Brooks, J. R., Kim, Y., & Meinzer, F. C. (2019). Investigating old-growth ponderosa pine physiology using tree-rings, δ 13 C, δ 18 O, and a process-based model. *Ecology*, *100*(6). https://doi.org/10.1002/ecy.2656

Venturas, M. D., Sperry, J. S., Love, D. M., Frehner, E. H., Allred, M. G., Wang, Y., & Anderegg, W. R. L. (2018). A stomatal control model based on optimization of carbon gain versus hydraulic risk predicts aspen sapling responses to drought. *New Phytologist*, *220*(3), 836–850. https://doi.org/10.1111/nph.15333

Venturas, M. D., Todd, H. N., Trugman, A. T., & Anderegg, W. R. L. (2021). Understanding and predicting forest mortality in the western United States using long-term forest inventory data and modeled hydraulic damage. *New Phytologist*, *230*(5), 1896–1910. https://doi.org/10.1111/nph.17043

Wang, Y., Sperry, J. S., Anderegg, W. R. L., Venturas, M. D., & Trugman, A. T. (2020). A theoretical and empirical assessment of stomatal optimization modeling. *New Phytologist*, *227*(2), 311–325. https://doi.org/10.1111/nph.16572

Webb, A. (1994). Principles of environmental physics. By J. L. Monteith & M. H. Unsworth. Edward Arnold, Sevenoaks. 2nd edition, 1990. Pp. Xii + 291. Price £15.99 (£32.00 hardback). ISBN 0 7131 2931 X. *Quarterly Journal of the Royal Meteorological Society*, *120*(520), 1700–1700. https://doi.org/10.1002/qj.49712052015

Williams, M., Rastetter, E. B., Fernandes, D. N., Goulden, M. L., Wofsy, S. C., Shaver, G. R., Melillo, J. M., Munger, J. W., Fan, S.-M., & Nadelhoffer, K. J. (1996). Modelling the soil-plant-atmosphere continuum in a Quercus–Acer stand at Harvard Forest: The regulation of stomatal conductance by light, nitrogen and soil/plant hydraulic properties. *Plant, Cell & Environment*, *19*(8), 911–927. https://doi.org/10.1111/j.1365-3040.1996.tb00456.x

Williams, M., Law, B. E., Anthoni, P. M., & Unsworth, M. H. (2001a). Use of a simulation model and ecosystem flux data to examine carbon-water interactions in ponderosa pine. *Tree Physiology*, *21*(5), 287–298. https://doi.org/10.1093/treephys/21.5.287

Williams, M., Rastetter, E. B., Shaver, G. R., Hobbie, J. E., Carpino, E., & Kwiatkowski, B. L. (2001b). Primary production of an arctic watershed: an uncertainty analysis. *Ecological*

Applications, *11*(6), 1800–1816. https://doi.org/10.1890/1051-0761(2001)011[1800:PPOAAW]2.0.CO;2

Williams, M., Schwarz, P. A., Law, B. E., Irvine, J., & Kurpius, M. R. (2005). An improved analysis of forest carbon dynamics using data assimilation. *Global Change Biology*, *11*(1), 89–105. https://doi.org/10.1111/j.1365-2486.2004.00891.x

Wolf, A., Anderegg, W. R., & Pacala, S. W. (2016). Optimal stomatal behavior with competition for water and risk of hydraulic impairment. *Proceedings of the National Academy of Sciences*, *113*(46), E7222-E7230.

Xu, X., Medvigy, D., Powers, J. S., Becknell, J. M., & Guan, K. (2016). Diversity in plant hydraulic traits explains seasonal and inter-annual variations of vegetation dynamics in seasonally dry tropical forests. *New Phytologist*, *212*(1), 80–95. https://doi.org/10.1111/nph.14009

Yang, J., Duursma, R. A., De Kauwe, M. G., Kumarathunge, D., Jiang, M., Mahmud, K., Gimeno, T. E., Crous, K. Y., Ellsworth, D. S., Peters, J., Choat, B., Eamus, D., & Medlyn, B. E. (2019). Incorporating non-stomatal limitation improves the performance of leaf and canopy models at high vapour pressure deficit. *Tree Physiology*, *39*(12), 1961–1974. https://doi.org/10.1093/treephys/tpz103

Zhou, S., Duursma, R. A., Medlyn, B. E., Kelly, J. W. G., & Prentice, I. C. (2013). How should we model plant responses to drought? An analysis of stomatal and non-stomatal responses to water stress. *Agricultural and Forest Meteorology*, *182–183*, 204–214. https://doi.org/10.1016/j.agrformet.2013.05.009

Journal of Advances in Modeling Earth Systems

Supporting Information for

Comparing model representations of functional controls on transpiration at a semi-arid Ponderosa Pine site

Linnia Hawkins[1], Maoya Bassouni[2], William R. L. Anderegg[3], Martin D. Venturas[4],

Stephen P. Good[5], Hyojung J. Kwon[1], Chad V. Hanson[1], Richard P. Fiorella[6],

Gabriel J. Bowen[6], and Christopher J. Still[1]

[1]Department of Forestry, Oregon State University, Corvallis, OR, [2]Department of Crop Production Ecology, Swedish University of Agricultural Sciences, Uppsala, Sweden, [3]University of Utah, Salt Lake, UT, [4]Departamento de Sistemas y Recursos Naturales, Universidad Politécnica de Madrid, Madrid, Spain, [5]Department of Biological and Ecological Engineering, Oregon State University, Corvallis, OR, [6]Department of Geology and Geophysics, Unversity of Utah, Salt Lake, UT

Contents of this file

Introduction

This supporting information file contains a text describing model updates (Text S1) and parameter sensitivity (Text S2), figures supporting the main text (S1 to S6).

Text S1. Updates made to the SPA model

Following Ruehr et al., (2014), we increased soil evaporation in the SPA model by lowering the tortuosity from 2.5 to 1.0 which increased soil conductance to water vapor diffusion. We further increased the soil conductance to water vapor diffusion by scaling the porosity in the top soil layer from 0.37 to 0.9. Lastly, we reduced the soil roughness length from 0.13 to 0.01 times the canopy height (18m).

As in Reuhr et al., (2014) a sigmoid function was added to scale aboveground tree conductance (gplant) by soil water potential (SWP) (eq. S1). We increased the sensitivity of gplant to SWP to improve model performance.

$$gplant = gplant_0 \left(0.2 + \frac{0.8}{(1+exp^{\left({}^{(SWP+0.784)}/_{0.163}\right)})} \right) \quad \text{(eq. S1)}$$

We also added an option to use site-specific soil water retention equations relating soil water content (SWC) to SWP in place of the widely used equations based on soil texture from Saxton et al., (1986). In this application, we used the following water retention relations from Ruehr et al., (2014):

$$SWP = -0.04 - \frac{1.6}{1+\exp\left(\frac{SWC-0.096}{0.0184}\right)} \quad \text{(eq. S2)}$$

Text S2. Parameter sensitivity analysis

For each model, 100 unique parameterizations were selected using a Latin hypercube sampling design (McKay et al., 1979). Two-year simulations were performed beginning January 1st, 2006 and ending December 31st, 2007 using each parameterization. The modeled transpiration (T) and gross primary productivity (GPP) were averaged over two growing seasons (May-July of 2006 and 2007) for each simulation (Figure S3). We performed a Fourier amplitude sensitivity test (FAST; Saltelli and Bolado, 1998) to quantify the contribution of each parameter to the total variance in

T across the perturbed parameter ensemble. For each parameter, the FAST quantifies the main effect as the ratio of an individual parameter's contribution to the total variance (Figure S4). Additionally, the proportion of variance contributed by interactions among parameters is quantified.

We identified the parameters most influential on the growing season mean transpiration for each model. The WUEi and WUE models were sensitive to the plant conductivity (gplant), which represents 39% and 22% of variance in seasonal mean T respectively (Figure S4). The minimum leaf water potential ($_{min}$LWP) was also influential, representing 45% of variance in the WUEi model and 26% of variance in the WUE model. The WUE model was more sensitive to the stomatal efficiency parameter than the WUEi model (33% and 9% respectively). The iota parameter determines the plant water use strategy; low values of iota allow plants to use water liberally in the mornings which can lead to water depletion and stomatal closure in the afternoons. High values of iota represent a more conservative water strategy, but often lead to lower total daily carbon gains.

In the Ball-Berry and Medlyn models the g_1 parameter is the dominant source of variability (Figure S4). The parameters influencing hydraulic limitations on stomatal conductance (eq. 6: *b* and *c*) have less impact on the variance in seasonal mean T. This is because hydraulic limitations only constrain the simulated T when soil water potential is low during the late summer (July-August). Transpiration rates during the early growing season are much higher and likely dominate the seasonal mean T. The range of values for the g_1 parameter is much larger (and thus much more influential on T) than the degree to which hydraulic limitation modifies g_1 for the latter half of the summer.

In the Sperry model, the maximum whole plant conductance parameter (K_{max}) is most influential on growing season mean T, followed by the *b* parameter in the leaf hydraulic vulnerability curve (eq. 7; $Weibull_b$). The K_{max} parameter determines the unstressed rate of T, but this parameter can be constrained with measurements (e.g., Love et al., 2018).

Given the functional form of the hydraulic vulnerability curve (eq. 7), the $Weibull_b$ parameter determines the point at which hydraulic conductivity falls to 50%, whereas the $Weibull_c$ parameter determines the steepness of the curve, i.e., how gradually the hydraulic conductivity falls to 50% of maximum conductivity. Given this relationship it is expected that perturbations to the $Weibull_b$ parameter are more influential on growing season mean T since it effectively determines how early in the summer T begins to be constrained by water availability. The leaf specific conductivity parameter (*LSC*) was not influential on growing season mean T (Figure S4).

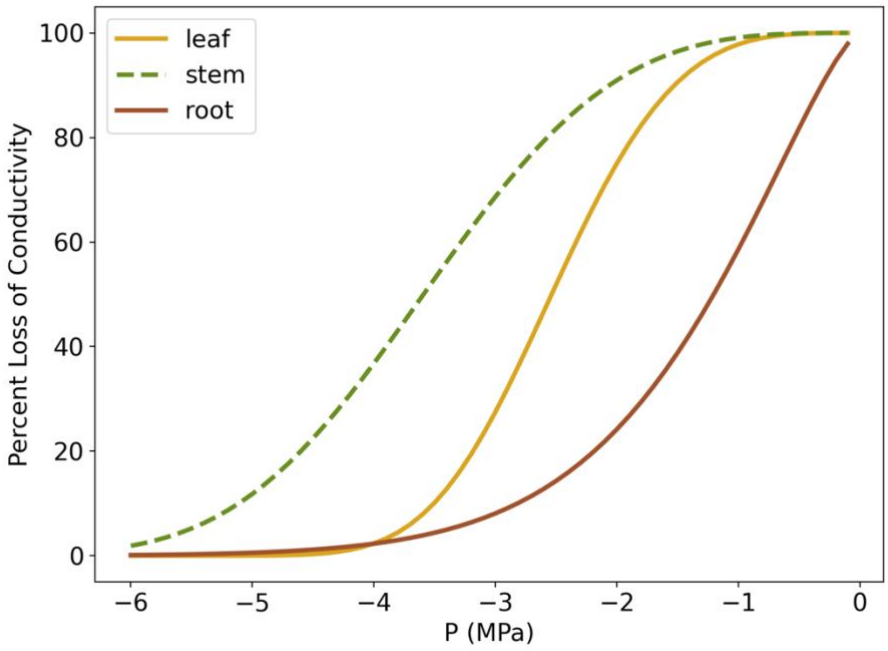

Figure S1. Hydraulic vulnerability curves (VC's) for leaves, stem, and roots used in the gain-risk model. The leaf VC is fit to ponderosa pine data from Johnson et al., (2009) as used in Sperry et al., (2019). The stem VC was measured at the US-Me2 site and agrees well with curves fit to data in Sperry et al., (2019). The root VC was fit to measurements from Stout & Sala, 2003, Domec et al., 2004, and Koepke & Kolb, (2013) as used in Sperry et al., (2019). The same leaf VC was used in the MED-H and BB-H models**.**

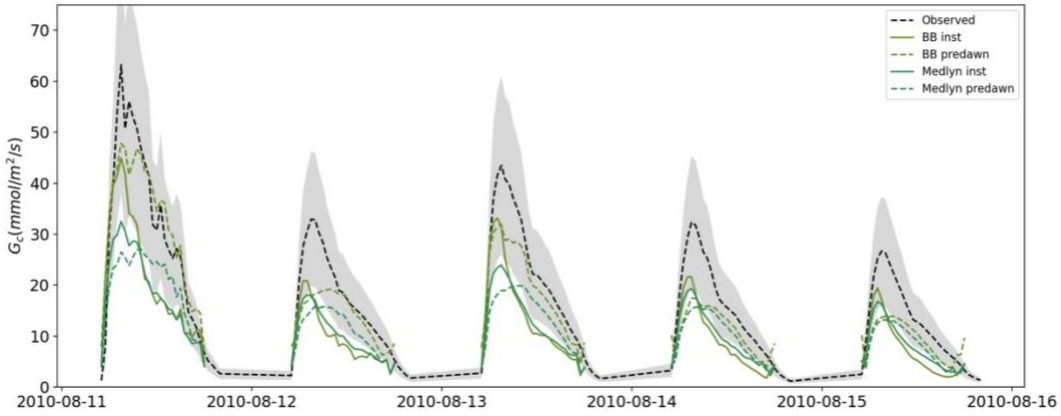

Figure S2. Simulated canopy conductance using the Ball-Berry and Medlyn models with hydraulic limitations based on instantaneous leaf water potential (solid) or predawn leaf water potential (dashed).

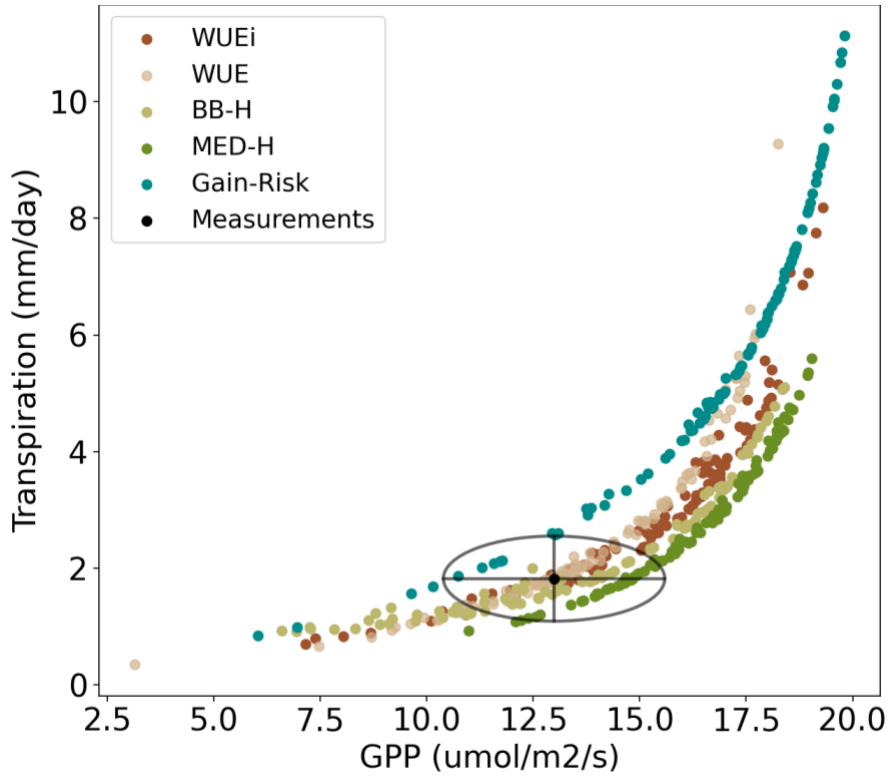

Figure S3. Model-simulated GPP (umol/m2/s) and transpiration (mm/day) during daytime averaged over the growing season (May-July) in 2006 and 2007 using 100 unique parameterizations. Observed GPP and T are shown in black with an oval representing measurement uncertainty. The non-linear relationship suggests that Rubisco limits GPP when transpiration rates are high, as opposed to stomatal limitation.

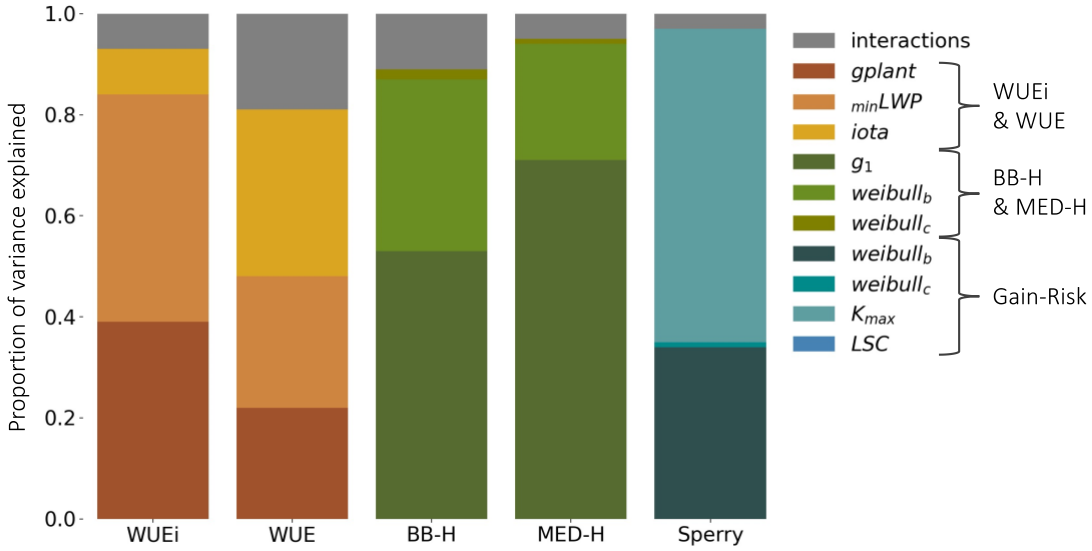

Figure S4. Proportion of the total emulated variance (total=1) in the 2006/2007 growing season mean transpiration contributed from perturbations of individual parameters, estimated with the Fourier Amplitude Sensitivity Test (FAST), and parsed into main effects (colors) and interaction terms among parameters (grey) for each model. Parameter sensitivity in the gain-risk model agrees well with previous studies (Venturas et al., 2018).

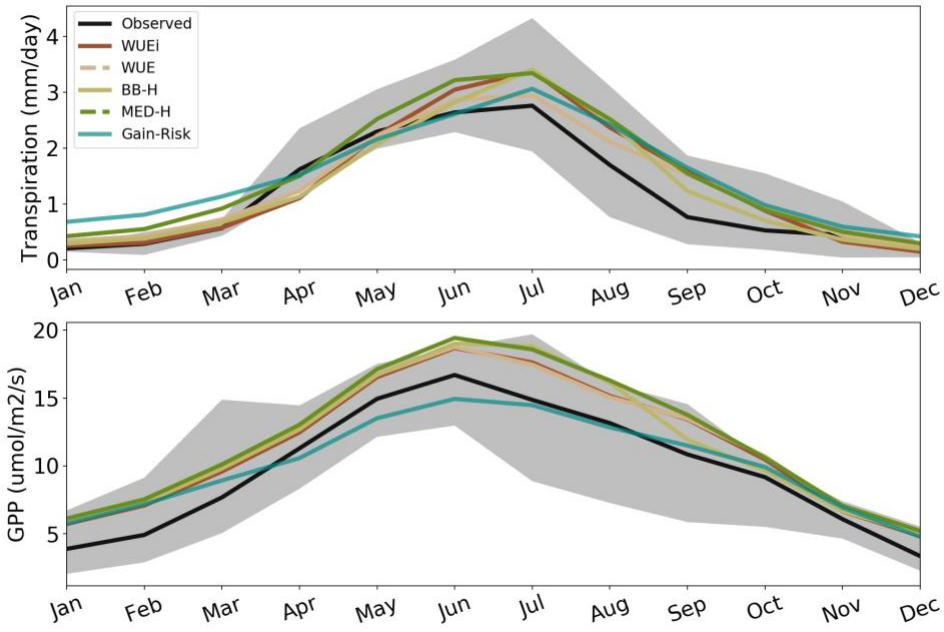

Figure S5. Mean annual cycle (2006–2018) of measured (black) and modeled (color) daytime (8am-4pm) transpiration (top; mm/day) derived from sapflow measurements and gross primary productivity (bottom; umol/m^2/s) from eddy-covariance measurements. Grey shading represents the range of observed monthly mean values from 2006–2018.

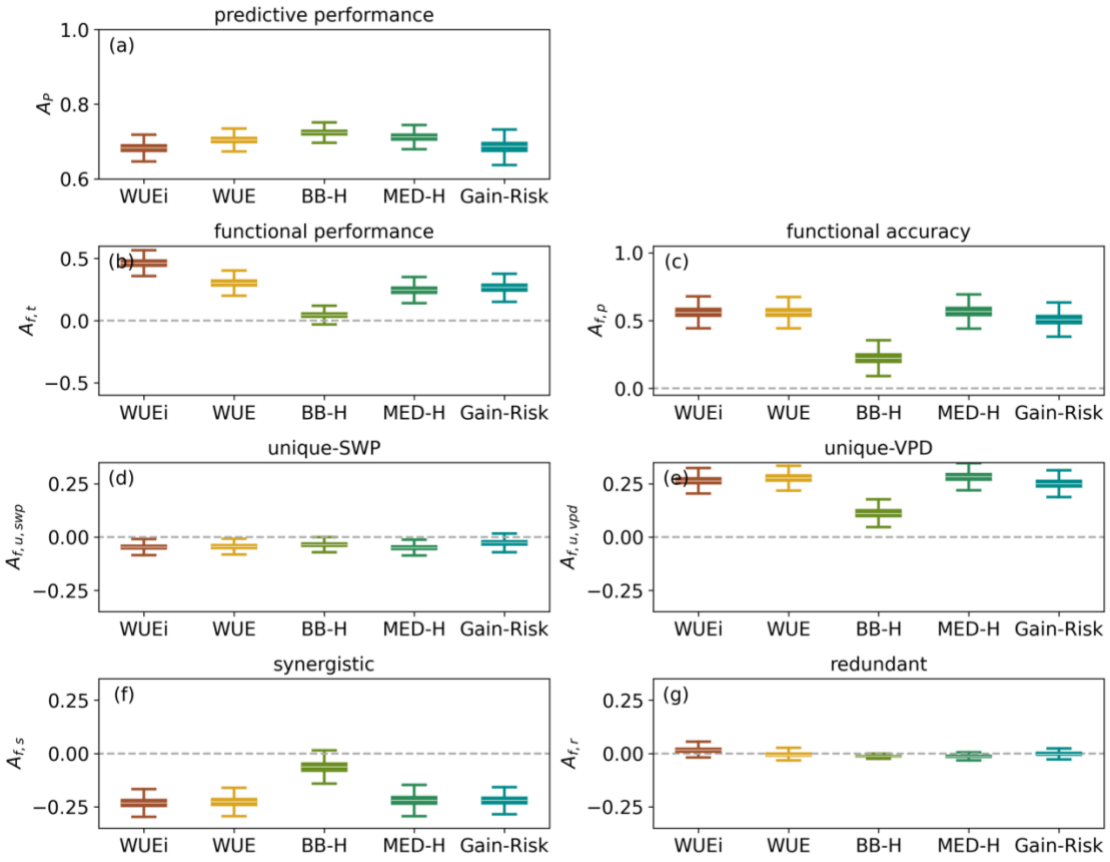

Figure S6. Evaluation of model predictive performance and information partitioning of daily transpiration (T) during growing season (May-August) of 2006 through 2018 when soil water potential (SWP) was above the 75th percentile (i.e., low soil water stress). (a) Predictive performance (A_P, bits bit-1) quantifies the relative fraction of information missing in the model about T compared to observations (a perfect model would have zero missing information). Boxes represent the interquartile range of bootstrapped samples; whiskers represent 5th and 95th percentiles; and white lines represent medians. (b) Functional performance; the relative difference between observed and modeled total multi-variate mutual information from SWP and VPD about T ($A_{f,T}$, bits bit-1). (c) Functional accuracy; the sum of multi-variate mutual information from SWP and VPD about T ($A_{f,P} = |A_{f,swp}| + |A_{f,VPD}| + |A_{f,S}| + |A_{f,R}|$, bits bit-1). The components of functional accuracy are partitioned into (d) unique from soil water potential ($A_{f,swp}$, bits bit-1), (e) unique from VPD ($A_{f,VPD}$, bits bit-1), (f) synergistic ($A_{f,S}$, bits bit-1), and (g) redundant ($A_{f,R}$, bits bit-1) information.